

Accepted Manuscript

From hit to lead: Structure-based discovery of naphthalene-1-sulfonamide derivatives as potent and selective inhibitors of fatty acid binding protein 4

Ding-Ding Gao, Hui-Xia Dou, Hai-Xia Su, Ming-Ming Zhang, Ting Wang, Qiu-Feng Liu, Hai-Yan Cai, Hai-Peng Ding, Zhuo Yang, Wei-Liang Zhu, Ye-Chun Xu, He-Yao Wang, Ying-Xia Li

PII: S0223-5234(18)30411-2

DOI: [10.1016/j.ejmech.2018.05.007](https://doi.org/10.1016/j.ejmech.2018.05.007)

Reference: EJMECH 10417

To appear in: *European Journal of Medicinal Chemistry*

Received Date: 27 February 2018

Revised Date: 4 May 2018

Accepted Date: 6 May 2018

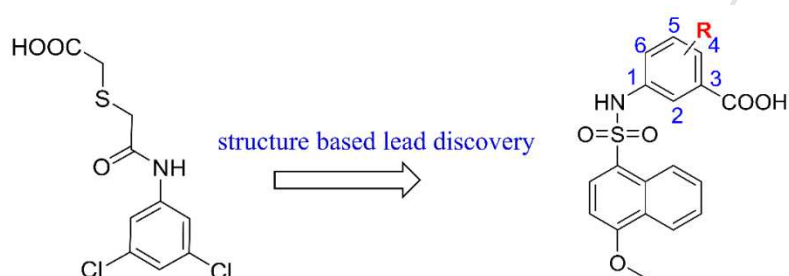
Please cite this article as: D.-D. Gao, H.-X. Dou, H.-X. Su, M.-M. Zhang, T. Wang, Q.-F. Liu, H.-Y. Cai, H.-P. Ding, Z. Yang, W.-L. Zhu, Y.-C. Xu, H.-Y. Wang, Y.-X. Li, From hit to lead: Structure-based discovery of naphthalene-1-sulfonamide derivatives as potent and selective inhibitors of fatty acid binding protein 4, *European Journal of Medicinal Chemistry* (2018), doi: 10.1016/j.ejmech.2018.05.007.

This is a PDF file of an unedited manuscript that has been accepted for publication. As a service to our customers we are providing this early version of the manuscript. The manuscript will undergo copyediting, typesetting, and review of the resulting proof before it is published in its final form. Please note that during the production process errors may be discovered which could affect the content, and all legal disclaimers that apply to the journal pertain.



From Hit to Lead: Structure-based Discovery of Naphthalene-1-Sulfonamide Derivatives as Potent and Selective Inhibitors of Fatty Acid Binding Protein 4

Ding-Ding Gao,[§] Hui-Xia Dou,[§] Hai-Xia Su,[§] Ming-Ming Zhang,[§] Ting Wang, Qiu-Feng Liu, Hai-Yan Cai, Hai-Peng Ding, Zhuo Yang, Wei-Liang Zhu,* Ye-Chun Xu,* He-Yao Wang,* and Ying-Xia Li *



9: FABP4, Ki: 1.66 μ M

16dk: 4-F, FABP4, Ki: 0.21 μ M

16do: 6-F, FABP4, Ki: 0.20 μ M

Good selectivity for FABP3

Good metabolic stabilities in liver microsomes

From Hit to Lead: Structure-based Discovery of Naphthalene-1-Sulfonamide Derivatives as Potent and Selective Inhibitors of Fatty Acid Binding Protein 4

Ding-Ding Gao,^{†,§} Hui-Xia Dou,^{‡,¶,§} Hai-Xia Su,^{#,¶,§} Ming-Ming Zhang,^{†,§} Ting Wang,[‡] Qiu-Feng Liu,[#] Hai-Yan Cai,^{#,△} Hai-Peng Ding,[†] Zhuo Yang,[#] Wei-Liang Zhu,^{*,#} Ye-Chun Xu,^{*,#} He-Yao Wang,^{*,‡} and Ying-Xia Li ^{*,†}

[†]School of Pharmacy, Fudan University, Shanghai 201203, China

[‡]State key Laboratory of Drug Research, Shanghai Institute of Materia Medica, Chinese Academy of Sciences, Shanghai 201203, China

[#]CAS Key Laboratory of Receptor Research; Drug Discovery and Design Center, Shanghai Institute of Materia Medica, Chinese Academy of Sciences (CAS), Shanghai 201203, China

[¶]University of Chinese Academy of Sciences, Beijing 100049, China

[△]Department of Pathophysiology, Key Laboratory of Cell Differentiation and Apoptosis of Chinese Ministry of Education, School of Medicine, Shanghai JiaoTong University, Shanghai 201203, China

*Corresponding Authors

E-mail addresses: liy417@fudan.edu.cn (Y. Li), hywang@simmm.ac.cn (H. Wang), yxcx@simmm.ac.cn (Y. Xu), wzhu@simmm.ac.cn (W. Zhu).

[§] These authors contributed equally to the work.

Abstract

Fatty acid binding protein 4 (FABP4) plays a critical role in metabolism and inflammatory processes and therefore is a potential therapeutic target for immunometabolic diseases such as diabetes and atherosclerosis. Herein, we reported the identification of naphthalene-1-sulfonamide derivatives as novel, potent and selective FABP4 inhibitors by applying a structure-based design strategy. The binding affinities of compounds **16dk**, **16do** and **16du** to FABP4, at the molecular level, are equivalent to or even better than that of BMS309403. The X-ray crystallography complemented by the isothermal titration calorimetry studies revealed the binding mode of this series of inhibitors and the pivotal network of ordered water molecules in the binding pocket of FABP4. Moreover, compounds **16dk** and **16do** showed good metabolic stabilities in liver microsomes. Further extensive *in vivo* study demonstrated that **16dk** and **16do** exhibited a dramatic improvement in glucose and lipid metabolism, by decreasing fasting blood glucose and serum lipid levels, enhancing insulin sensitivity, and ameliorating hepatic steatosis in obese diabetic (*db/db*) mice.

Keywords: FABP4 inhibitors, FABP3 sparing, Structure-based design strategy, X-ray crystallography.

■ Introduction

Lipids are critical modulators that regulate the metabolic, inflammatory and innate immune processes in intracellular and extracellular signaling coordinately [1]. As intracellular lipid chaperones or fatty acids shuttles, fatty acid binding proteins (FABPs) are a family of 14–15 kDa proteins that modulate lipid fluxes, trafficking and signaling, and thus play important roles in lipid metabolism and inflammation. At least ten members have been identified since the initial discovery of FABPs in 1972. Each of them exhibits tissue-specific distribution and is expressed richly in tissues associated with active lipid metabolism (LFABP or FABP1, liver; IFABP or FABP2, intestines; HFABP or FABP3, heart; AFABP or FABP4, adipocyte; EFABP or FABP5, epidermis; IIFABP or FABP6, ileum; BFABP or FABP7, brain; MFABP or FABP8, myelin; TFABP or FABP9, testis; LOC646486 or FABP12, Human retinoblastoma cell lines) [2-6]. It is intriguing that these members possess only moderate sequence homology ranging from 15% to 70%, but their overall 3-D structures are very similar [2,7,8].

Fatty acid binding proteins 4 (also known as AFABP or aP2) is highly expressed in differentiated adipocytes, macrophages and endothelial cells, and induced by insulin and/or insulin-like growth factors-1 (IGF-1), fatty acids, as well as peroxisome-proliferator-activated receptor- γ (PPAR- γ) agonists [9-12]. Epidemiological studies and animal knockout models showed that FABP4 is crucial to in many aspects of metabolic syndrome. For example, FABP4^{-/-} mice were protected from obesity-induced insulin resistance, cardiovascular disease and hyperglycaemia [13,14]. Ablation of FABP4 in apolipoprotein E (ApoE)-deficient mice showed protection from atherosclerosis [11]. Additionally, the FABP4-deficient mice show reduced lipolysis but increased lipogenesis [15]. FABP4 plays also an important role in carcinogenesis, such as ovarian, prostate, bladder, breast, renal cell carcinoma and other types of cancer cells [16]. FABP3, another important member of the FABPs family, is mainly expressed in cardiac as well as skeletal muscle tissues and has important roles in cell proliferation, apoptosis and prevention of oxidative stress. Silencing of FABP3 in embryonic carcinoma cells led to reduced proliferation and promoted apoptosis [17]. Also, specific deletion of cardiac muscle FABP3 in zebrafish resulted in apoptosis-induced mitochondrial dysfunction and impairment of cardiac development [18,19]. Accordingly, selective inhibition of FABP4 without disruption of FABP3 is an important precondition to develop druggable FABP4 inhibitors for the treatment of metabolic syndromes, such as obesity, insulin resistance, diabetes, and atherosclerosis.

To date, several classes of FABP4 inhibitors have been identified and exhibited good inhibitory potency, for example, pyrazole derivatives (**1**), quinoline derivatives (**2**), indole derivatives (**3**),

pyrimidine derivatives (**4**), thiophene derivatives (**5**), oxazole and imidazole derivatives (**6**, **7**), 1,3,5-triisopropylbenzene derivatives (**8**) (Fig. 1) [20-28]. Among which, pyrazole compound **1** has been utilized as a chemical tool for FABP4 inhibition both *in vitro* and *in vivo* [20]. In our previous study, compound **9** bearing 2-((2-oxo-2-(phenylamino)ethyl)thio)acetic acid scaffold, with an IC_{50} value of 13.5 μ M (K_i : 1.66 μ M) against FABP4, was discovered by virtual screening [27]. Molecular dynamics (MD) simulation and site-directed mutagenesis studies were carried out to identify the binding pattern. Taking compound **9** as a hit to perform a structural optimization and SAR study led us to design more potent inhibitors bearing naphthalene-1-sulfonamide scaffold. Furthermore, the X-ray crystal structures combined with isothermal titration calorimetry (ITC) revealed the binding mode of compounds **16d**, **16dk**, **16do**, **16di** with FABP4. We also performed a systematic study to validate the potency and efficacy of **16dk** and **16do** both *in vitro* and *in vivo*, respectively.

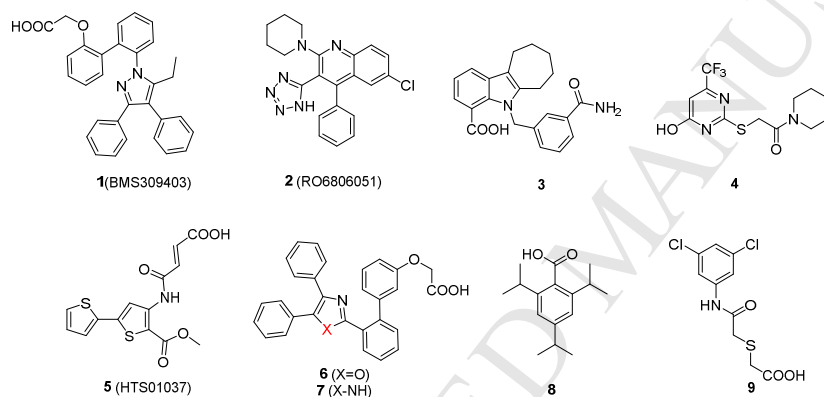
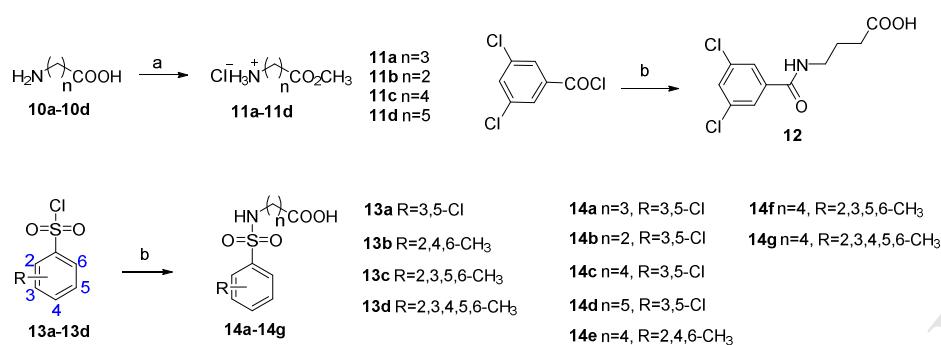


Fig. 1. Structures of representative FABP4 inhibitors.

■ Results and discussion

Chemistry

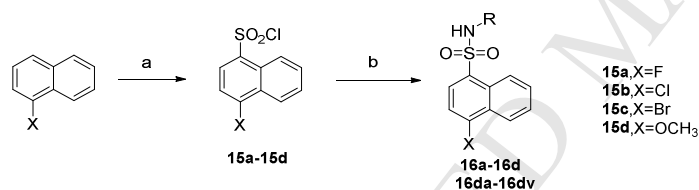
Methods for the synthesis of compounds **12** and **14a-14g** were outlined in Scheme 1. Commercially available **10a-10d** were transformed to corresponding amino acid methyl ester hydrochlorides **11a-11d** in good yields with the thionyl chloride/ CH_3OH system. Then the desired compounds (**12**, **14a-14g**) were obtained through a two-step consecutive reaction. Treatment of the intermediates **11a-11d** with 3,5-dichlorobenzoyl chloride or substitutive benzenesulfonyl chloride in dichloromethane at room temperature resulted in the formation of corresponding product precursors. Subsequent sodium hydroxide hydrolysis of the esters gave compounds **12** and **14a-14g**.



Reagents and conditions: (a) SOCl_2 , CH_3OH , 0°C to rt; (b) (i) **11a-11d**, CH_2Cl_2 , pyridine, 0°C to rt. (ii) NaOH , H_2O , CH_3OH , rt.

Scheme 1. Synthesis of Compounds **12**, **14a-14g**

Compounds **16a-16d** and **16da-16dv** were synthesized as described in Scheme 2. The reaction of commercially available naphthalene derivatives with chlorosulfonic acid in chloroform led to the formation of the corresponding naphthalene-1-sulfonyl chlorides (**15a-15d**), which were further reacted with **11c** or amino derivatives using the same method as the synthesis of compound **12**.



^a Reagents and conditions: (a) ClSO_2OH , CHCl_3 , 0°C to rt; (b) (i) **11c** or amino derivatives, CH_2Cl_2 , pyridine, 0°C to rt. (ii) NaOH , H_2O , CH_3OH , rt.

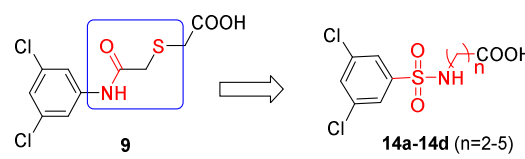
Scheme 2. Synthesis of compounds **16a-16d**, **16da-16dv**

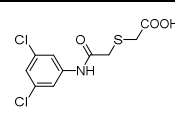
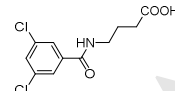
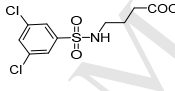
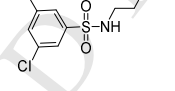
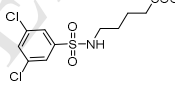
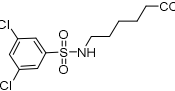
Hit optimization and identification of compounds **16dk** and **16do**.

From our reported binding mode of compound **9** (hit) with FABP4 protein, the aromatic ring is located in a large hydrophobic region made of Y19, M20, V23, V25, A33, F57, and A75. Also, it interacts with the electron-rich phenyl ring of F16 via π - π stacking and the carboxylic acid group makes polar interactions with R126 and Y128 (Fig. S4) [27]. In an effort to obtain more potent FABP4 inhibitors, the structure optimization was first focused on the linker between the carboxylic acid and the aromatic ring of hit compound **9**, and the results were shown in Table 1. Reversing the amide and replacing the sulfur atom with a carbon atom obtained the compound **12** of which the K_i value is $4.32\ \mu\text{M}$, worse than that of compound **9** (K_i : $1.66\ \mu\text{M}$). Interestingly, the activity is slightly improved when the amide

(**12**) was changed into a sulfonamide (**14a**, K_i : 2.55 μM). Subsequently, the length of the aliphatic chain of **14a** was explored and compound **14c** (K_i : 1.19 μM) with four carbon atoms between the sulfonamide and the carboxylic acid group was more potent than compounds **14a**, **14b** and **14d** (Table 1).

Table 1. Inhibitory activities of designed compounds



Compd.	Structure	K_i (μM) ^a
9		1.66±0.19
12		4.32±0.36
14a		2.55±0.32
14b		6.51±0.31
14c		1.19±0.01
14d		4.84±0.36
1		0.35±0.04

^a Each compound was tested in triplicate and the data are presented as the mean \pm SD.

Molecular docking (Schrodinger, Maestro suite) of compound **14c** with FABP4 (PDB code: 2HNX) showed that the aromatic ring was located in a large hydrophobic region and the carboxylate makes H-bonding interactions with R126 and Y128 (Fig. 2A). Additionally, one oxygen atom of the sulfonamide group forms additional two H-bonds with R78 and Q95. We envisioned that the introduction of more hydrophobic groups on the phenyl ring or using bulkier hydrophobic fragment may improve the potency. To validate our hypothesis, a series of sulfonamide compounds were

designed and synthesized, and their inhibitions to FABP4 were tested. As summarized in Table 2, introducing more methyl groups on the phenyl ring was favorable, as the K_i value of **14e**, **14f** and **14g**, with three, four and five methyl groups, respectively, is gradually decreased. Replacement of the phenyl ring with a naphthyl ring further improved the hydrophobic interaction. It's interesting that the substitution at the C-4 position of the naphthyl ring has a remarkable effect on target inhibition. Compared to compound **16a** (K_i : 2.16 μM) with a fluorine substitution, the inhibitory activities increased when a chlorine (**16b**, K_i : 1.85 μM), a bromine (**16c**, K_i : 1.16 μM), or a methoxy group (**16d**, K_i : 0.59 μM) was introduced at this position.

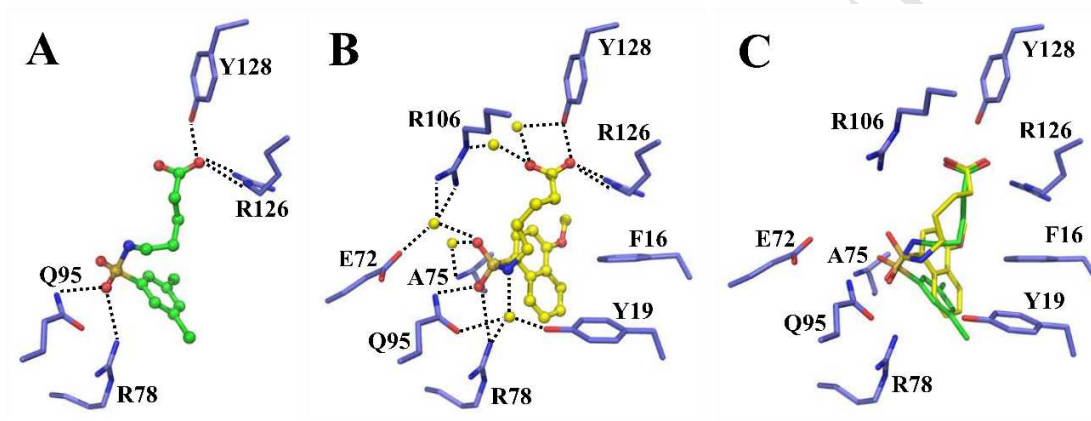
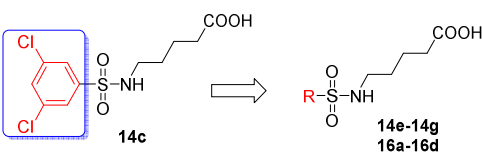
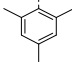
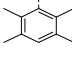
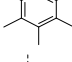
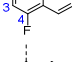
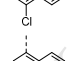
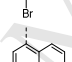
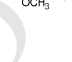


Fig. 2. (A) The predicted binding mode of compound **14c** with FABP4 resulted from a molecular docking (PDB code: 2HNX). (B) The X-ray crystal structure of FABP4 in complex with compound **16d** (PDB code: 5Y12). (C) An overlay of the predicted binding mode of compound **14c** (green) with the complex structure of FABP4-**16d** (yellow). The dashed lines in black represent hydrogen bonds.

Table 2. Inhibitory Activities of Designed Compounds


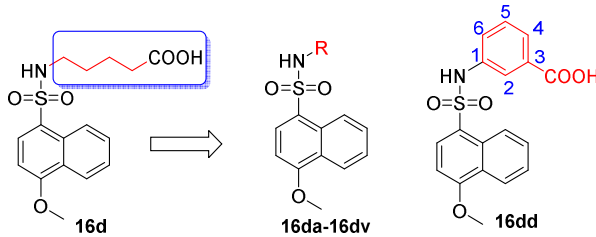
Compd.	R	K _i (μM) ^a
14e		2.69±0.07
14f		1.95±0.17
14g		0.91±0.11
16a		2.16±0.00
16b		1.85±0.18
16c		1.16±0.07
16d		0.59±0.03
1		0.35±0.04

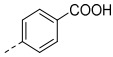
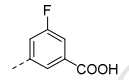
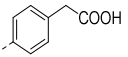
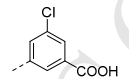
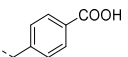
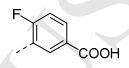
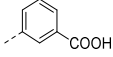
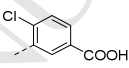
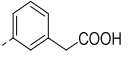
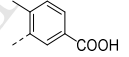
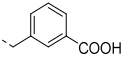
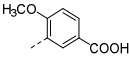
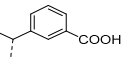
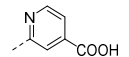
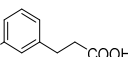
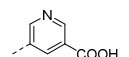
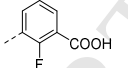
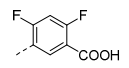
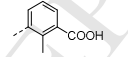
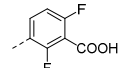
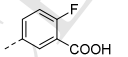
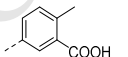
^a Each compound was tested in triplicate and the data are presented as the mean ± SD.

To further elucidate the binding modes of this series of inhibitors, the high-resolution crystal structures of FABP4 in complex with compound **16d** were solved (PDB code 5Y12). As depicted in Fig. 2B, the naphthyl ring of compound **16d** occupies the large hydrophobic pocket and forms edge-to-face π -stacking interactions with the phenyl ring of F16. The carboxyl group is engaged in direct H-bonds with R126 and Y128, together with two water-mediated H-bonds with R106 and Y128. In particular, the sulfonamide group participates in many H-bonding interactions with neighboring residues. In detail, one oxygen atom of the sulfonamide group forms H-bonds with R78 as well as Q95, and the second oxygen establishes a few water-bridged H-bonds with E72, A75 and R106. Besides, through a water molecule, the NH group make H-bond interactions with residues Y19, R78 and Q95.

Guided by the crystal structures of FABP4 in complex with compound **16d**, we further focused on modifying the aliphatic chain moiety and the electronic nature of the carboxyl group. In the first step, all or partial of the aliphatic chain moiety was replaced with a benzene ring to reduce the flexibility

(**16da-16dh**) so as to increase the compounds' binding affinities against FABP4 (Table 3). The carboxyl or carboxymethyl placed at the meta-position of the phenyl ring was better than at the para-position (**16da** vs **16dd**, **16db** vs **16de**). Changing the para-carboxylphenyl group (**16da**) into a para-carboxylbenzyl one (**16dc**) improved the binding affinity from 1.28 μM to 0.76 μM , while replacing the meta-carboxylphenyl group (**16dd**) with a meta-carboxylbenzyl one (**16df**) or its derivative (**16dg**) led to decreased binding affinity. In comparison with **16de**, the addition of a methylene between the phenyl ring and the carboxyl group (**16dh**) slightly increased the binding affinity which indicated that the length of methylene and activities did not correlate very well. Next, on the basis of the most potent compound **16dd**, structural variations were conducted by mainly introducing electron-donating or -withdrawing groups on the phenyl ring to change the electronic property of the carboxyl group (Table 3). Interestingly, only the small electron-withdrawing fluorine atom at the C-4 (**16dk**, K_i : 0.21 μM) or C-6 (**16do**, K_i : 0.20 μM) position led to improvement of the activities due to the increased salt bridge interaction between the carboxyl group and R126. The larger electron-withdrawing group (6-Cl, **16dp**; 6-OCH₃, **16dr**) or electron-donating group (4-CH₃, **16dl**; 6-CH₃, **16dq**) at these positions resulted in decreased binding affinities, suggesting that steric clashes of these substitutions with residues might occur. Moreover, the attachment of two fluorine substituents at both the C-4 and C-6 positions (**16du**) failed to increase the binding affinity compared to compounds **16dk** and **16do**. When the fluorine or chlorine was attached to the C-5 position (**16dm** and **16dn**), their binding affinity were 2-3-fold less potent compared with **16dd**. Replacing the benzene ring with an electron-poor aromatic system such as a pyridine ring (**16ds** and **16dt**) also reduced the binding affinity dramatically. Intriguingly, neither the small electron-withdrawing fluorine atom (**16di** and **16dv**) nor the electron-donating group (**16dj**) at the C-2 position resulted in more potent compounds. All of these results indicated that the pyridine ring or a big substitution at the phenyl moiety was not tolerable. The replacement of a fluorine atom at the C-4 or C-6 position of the phenyl resulted in compounds (**16dk** and **16do**) with higher potency than **1**, but it is detrimental when the fluorine was placed at the C-2 or C-5 position.

Table 3. Inhibitory activities of designed compounds


Compd.	R	K _i (μM) ^a	Compd.	R	K _i (μM) ^a
16da		1.28±0.03	16dm		1.15±0.09
16db		1.67±0.02	16dn		0.82±0.01
16dc		0.76±0.02	16do		0.20±0.01
16dd		0.40±0.02	16dp		0.93±0.01
16de		0.84±0.02	16dq		2.76±0.09
16df		2.12±0.07	16dr		>6.14
16dg		>6.14	16ds		>6.14
16dh		0.58±0.01	16dt		>6.14
16di		7.75±0.09	16du		0.23±0.01
16dj		>6.14	16dv		7.38±0.15
16dk		0.21±0.01	1		0.35±0.04
16dl		>6.14			

^a Each compound was tested in triplicate and the data are presented as the mean ± SD.

Structural and thermodynamic characterization of 16dk, 16do and 16di binding to FABP4

To understand why incorporation of a fluorine atom at the C-4 or C-6 position of the phenyl ring was favorable while it was detrimental with the 2-fluorinated benzene, the complex structures of FABP4 with **16dk**, **16do** and **16di** (PDB code: **16dk**, 5Y0F; **16do**, 5Y0G; **16di**, 5Y0X) were determined. As depicted in Fig. 3, the naphthyl and sulfonamide group of these three inhibitors formed the similar

interactions with FABP4 as those found with compound **16d**. Furthermore, compounds **16dk** and **16do** which possess a fluorine atom at the C-4 position or the C-6 position of the phenyl ring have the same binding mode within FABP4. However, the orientation of the phenyl ring of compound **16di** shifted due to the introduction of a fluorine at the C-2 position in this compound (Fig. 3A). We speculated that the 2-F substituent had clashes with the oxygen atom of the sulfonamide group, which led to the changed orientation of the phenyl. To test this, we added a fluorine atom to the C-2 position of compound **16dk** in silico, and the resulting distance between the added fluorine and one oxygen atom of the sulfonamide group was 2.3 Å (Fig. S3). Given the high electronegativity of both oxygen and fluorine and the sum of the Van der Waals radius of two atoms (2.99 Å), the orientation of the phenyl had to be altered to avoid the repulsive force as well as clashes between two atoms. Such an orientation change of the phenyl ring caused the side-chain movement of R126 together with F16, as cation- π interactions are formed between these two residues (Fig. 3B). The side-chain movement of R126 weakened its H-bonding interactions with the carboxyl oxygen of **16di**. Notably, a network of the ordered water molecules surrounding compound **16do** was disrupted in the complex of FABP4 bound with **16di** (Fig. 3C and 3D). In comparison with the network in the complex structures of FABP4-**16dk** and FABP4-**16do**, three water molecules around the carboxyl group disappeared in the complex of FABP4-**16di**, resulting that the H-bonding interactions between the carboxyl oxygen of **16di** and R106 was thus broken. This together with the weakened H-bond between R126 and the carboxyl oxygen may explain why the binding affinity of **16di** to FABP4 was reduced compared to that of **16dk** or **16do**.

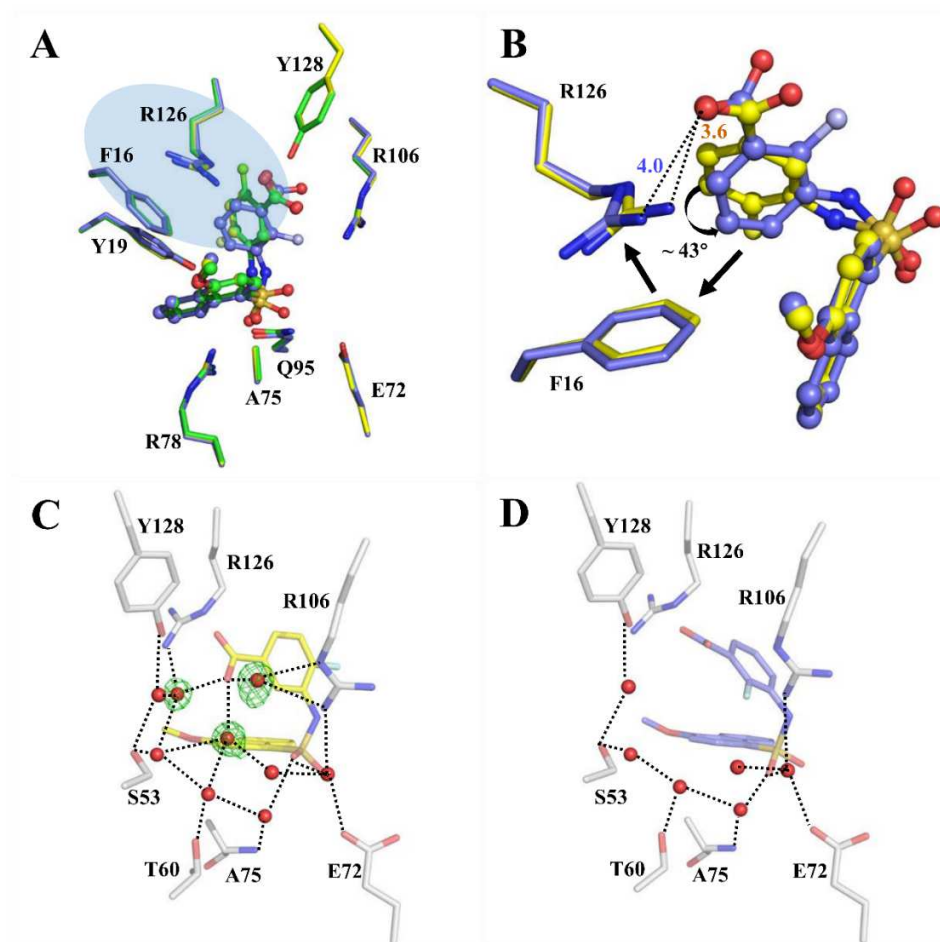


Fig. 3. X-ray structures of FABP4 in complex with compounds **16dk** (green) (PDB code: 5Y0F), **16do** (yellow) (PDB code: 5Y0G) and **16di** (blue) (PDB code: 5Y0X). (A) An overlay of complex structures of FABP4-**16dk**, FABP4-**16do** and FABP4-**16di**. Residues are shown in stick. Inhibitors are shown in ball and stick. The light blue shadow marks the change of the phenyl ring and the adjacent residues with a shifted side-chain. (B) The superimposed structures of the FABP4-**16do** and FABP4-**16di** complexes. (C) A critical water network in the complex structure of FABP4-**16do**. The water molecules are shown in red sphere. (D) The disrupted water network in the complex structure of FABP4-**16di**.

To gain more insight into how the changes of the phenyl ring orientations as well as the surrounding water network affected the binding free energy [31,32], thermodynamic properties of **16di** and **16do** binding to FABP4 in solution was investigated by ITC measurements. The averaged dissociation constant (K_d), binding free energy (ΔG), enthalpy (ΔH), and entropy term ($-T\Delta S$) resulted from three independent ITC measurements on each compound were listed in Table 4. Consistent with the different binding patterns revealed by the complex structures, compound **16di** and **16do** displayed

significantly different binding thermodynamics. The multiple H-bonding as well as hydrophobic interactions of **16do** with the protein is in accord with the huge enthalpy (ΔH : -59.64 kJ/mol) resulted from the ITC measurements, while it is much less for **16di** (ΔH : -25.87 kJ/mol) due to, as mentioned above, the less interactions formed between **16di**, in particular the carboxyl group, and FABP4. Although the binding of both compounds with FABP4 were mainly driven by the enthalpic term, the entropy contribution to their binding were just opposite for two compounds. Binding of compound **16do** to FABP4 exhibited a substantial entropic penalty ($-T\Delta S$: 25.72 kJ/mol), whereas in the case of **16di** the complex formation benefited from the entropic effect ($-T\Delta S$: -4.38 kJ/mol). Accordingly, the binding free energies for two compounds are close to each other, but the enthalpic and entropic contributions to the binding in two cases are distinctive. In comparison with **16do**, the lower binding enthalpy and positive contribution of the entropy for **16di** binding to FABP4 could be ascribed to the disruption of the H-bonds and the water-molecule-network resulted from the orientation change of the phenyl ring, and the releasing of three ordered water molecules from the network.

Table 4. Thermodynamic parameters of **16di** and **16do** binding to FABP4

Compd.	K_d (M) ^a	ΔG (kJ/mol) ^a	ΔH (kJ/mol) ^a	$-T\Delta S$ (kJ/mol) ^a
16di	$(6.03 \pm 0.31) \times 10^{-6}$	-30.25 ± 0.13	-25.87 ± 0.15	-4.38 ± 0.02
16do	$(1.40 \pm 0.07) \times 10^{-6}$	-33.92 ± 0.13	-59.64 ± 0.53	25.72 ± 0.66

^a Each compound was tested in triplicate and the data are presented as the mean \pm SD.

The selectivity of representative compounds against FABP3 and other fatty acid targets

As FABP3 has important roles in cell proliferation, apoptosis and prevention of oxidative stress in cardiac and red skeletal muscle tissues [17], the selectivity between FABP3 and FABP4 is a crucial issue for design of FABP4 inhibitors. Therefore, the inhibition of four compounds, which have good binding affinity to FABP4, to FABP3 were examined and listed in Table 5. Remarkably, our compounds showed a good selectivity of FABP4 over FABP3. It is even better than the selectivity of **1** and **2** to FABP3. We then superimposed the crystal structure of **16do** bounded FABP4 with the structure of FABP3 in complex with the palmitic acid to exploit the difference in the ligand binding sites. As shown in Fig. 4, the sub-pocket for the phenyl ring of **16do** includes residues V115 and C117 in FABP4 but the corresponding residues in FABP3 are L115 and L117, with a larger side-chain. It seems that compound **16do** would have clashes with these two amino acids in FABP3. Therefore, the inappropriate complementarity between the compound and the ligand binding pocket of FABP3 accounts for the weaker FABP3 activity of **16do**. Moreover, the selectivity of compounds **16dk** and **16do** on other fatty acid targets was evaluated to exclude the off-target effects. The results show that

none of them exhibit activity towards GPR40 (Free fatty acid receptor 1), GPR120 (Free fatty acid receptor 4), DGAT1 (Acyl coenzyme A: diacylglycerol acyltransferase 1) and PPAR γ (Peroxisome proliferator activated receptor γ) (see Table S3).

Table 5. Selectivity of representative compounds against FABP3

Compd.	FABP4 K _i (μ M) ^a	FABP4 IC ₅₀ (μ M) ^a	FABP3 IC ₅₀ (μ M) ^a	FABP3/FABP4
16dd	0.40 \pm 0.02	3.22 \pm 0.17	>100	>31
16dk	0.21 \pm 0.01	1.69 \pm 0.12	>100	>59
16do	0.20 \pm 0.01	1.65 \pm 0.12	>100	>60
16du	0.23 \pm 0.01	1.84 \pm 0.10	>100	>54
1	0.35 \pm 0.04	2.82 \pm 0.35	40.83 \pm 3.27	14.5
2	0.087 \pm 0.002	0.71 \pm 0.06	4.6 \pm 0.41	6.5

^a Each compound was tested in triplicate and the data are presented as the mean \pm SD.

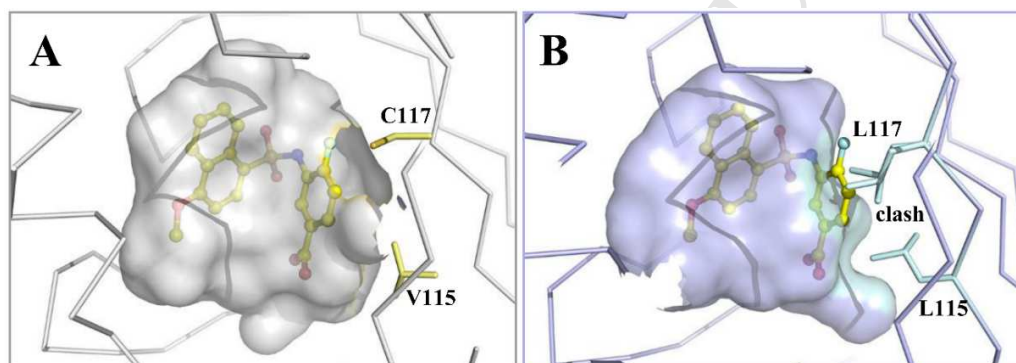


Fig. 4. (A) The binding mode of Compound **16do** in the pocket of FABP4 (PDB code: 5Y0G). (B) The superimposed structures of the FABP4-**16do** complex and FABP3 (PDB code 4TKB). **16do** and the structure of FABP3 were shown. The ligand binding pockets are shown with their inter-molecular surface.

Effects of **16dk** and **16do** on adipocytes.

It has been reported that genetic ablation or pharmacological inhibition of FABP4 can inhibit lipolysis and increase lipogenesis in adipocytes [15,33]. To investigate the effects of **16dk** and **16do** on adipocytes, lipolysis assay, triglyceride assay and oil red staining were carried out one by one. Firstly, the cytotoxicity of **16dk** and **16do** were tested using MTT assay. As illustrated in Fig. S1, they had no significant cytotoxicity up to 80 μ M in 3T3-L1 pre-adipocytes while **1** at a concentration of 80 μ M caused the death of \sim 50% cells. As shown in Fig. 5A, both compounds reduced glycerol levels in mature adipocytes supernatants at 25 μ M and 50 μ M, exhibiting an inhibition of forskolin-stimulated lipolysis in a dose-dependent manner. They also significantly increased intracellular triglyceride content (Fig. 5B) and lipid droplets (Fig. 5C and 5D) during adipocytes differentiation. The above

results suggested that both **16dk** and **16do** could inhibit lipolysis and enhance lipid accumulation. These results are in agreement with the inhibitory activity data of **16dk** and **16do** on FABP4 and consistent with the phenotypes of targeted FABP4 deletion in adipocytes, which further confirm that **16dk** and **16do** are FABP4 inhibitors.

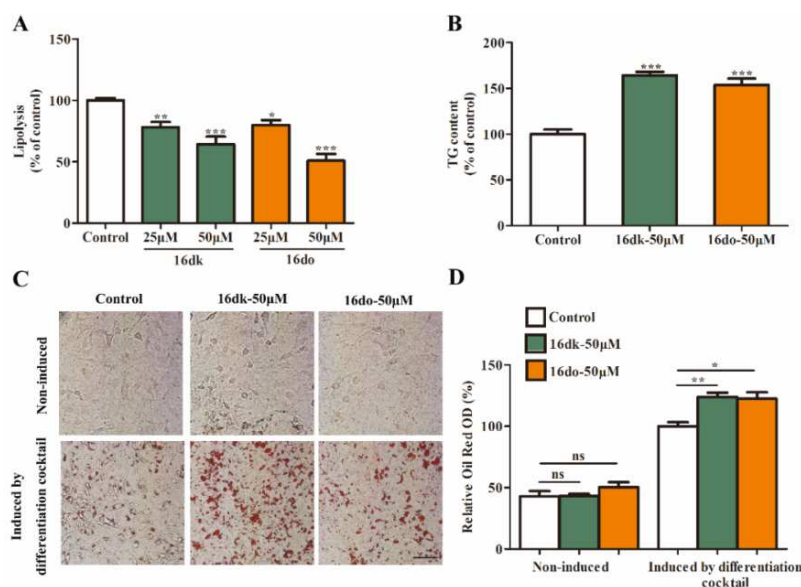


Fig. 5. Compounds **16dk** and **16do** inhibit lipolysis and increase lipid accumulation. (A) Effect of compounds **16dk** and **16do** on the release of free glycerol from forskolin-stimulated mature 3T3-L1 adipocyte. Fully differentiated 3T3-L1 were incubated with either DMSO (control) or compounds **16dk** and **16do** (25 μM and 50 μM) for 24 hours, then the supernatant was collected and its glycerol level was measured by an assay kit. (B, C, D) Effect of compounds **16dk** and **16do** on the lipid accumulation during differentiation. DMSO (control), **16dk** and **16do** (50 μM) were added with differentiation induction media in the whole differentiation period. At day 6, intracellular triglyceride was measured and oil red staining followed by quantification of the extracted oil red dye were performed (Scale bar =20 μm). * $p < 0.05$, ** $p < 0.01$, *** $p < 0.001$ vs. control group. Values are presented as mean \pm S.E.M from three independent experiments (n = 3).

Stabilities of **16dk** and **16do** tested with *in vitro* microsomes

The stabilities of compounds **16dk** and **16do** in microsome were evaluated using liver microsome preparations from mouse, rat, and human. It shows that both compounds were very stable in microsomes (Table 6). The percentage of the parent remaining was more than 90% in rat and mouse microsomes after 60 min. More than 70% of parent compounds were maintained after metabolism in human liver microsome. Furthermore, both compounds metabolized slowly with $T_{1/2}$ values ranging from 4.66 to 24.6 h and showed low CL_{int} in all species. All of these data indicate that compounds

16dk and **16do** have good metabolic stabilities in liver microsomes.

Table 6. Microsome stability of 16dk and 16do.

Compd.	Species	T _{1/2} (h)	Cl _{int} (mL/min/gprot)	% parent @ 60 min ^a
16dk	Human	4.66	7.51	72.3
16dk	Rat	11.1	3.15	93.4
16dk	Mouse	24.6	1.4	96.9
16do	Human	4.99	7.02	73.6
16do	Rat	12.1	2.90	93.9
16do	Mouse	14.3	2.4	94.8

^a Mean percentage remaining of parent compounds (0.1 μM) 60 min after incubation with the indicated liver microsomes.

***In vivo* efficacy of 16dk and 16do**

The leptin receptor-deficient *db/db* mice, with severe obesity and insulin resistance, and their lean littermates C57/BL6 were used to investigate the effect of **16dk** and **16do** on glucose, lipid metabolism and insulin sensitivity. As shown in Fig. S2, oral administration of **16dk** and **16do** did not show significant body weight loss and observable abnormalities of main organs such as liver, kidney and pancreas, and relative lipid content of abdominal adipose tissue at a dose of 100 mg/kg for a period of 5-week treatment. In contrast, the weekly fasting blood glucose levels of **16dk** and **16do** treated-groups were decreased 20-35% (Fig. 6A). Glucose area under the curve (AUC) during glucose tolerance tests (OGTT) in all groups after 2- and 4-week compounds treatment reduced significantly compared with the vehicle group, revealing a significant improvement in glucose metabolism (Fig. 6B-E). Insulin tolerance tests (ITT, Fig. 6F) along with the western blot (Fig. 8B) resulted in significantly increased insulin sensitivity in the *db/db* mice treated with **16dk** and **16do**. Additionally, compounds **16dk** and **16do** could reduce the serum levels of ALT and AST (Fig. 7A and 7B), two liver enzymes indicating liver damage, indicating an improvement of the compounds on liver function. Furthermore, **16dk** and **16do** treatment also significantly decreased serum levels of triglyceride (TG) and non-esterified fatty acid (NEFA) (Fig. 7C and 7E), suggesting the favorable effect of the compounds on lipid metabolism. However, the level of total cholesterol (TCH) was almost unchanged (Fig. 7D). Compared with the lean mice, the vehicle-treated *db/db* mice exhibited severe hepatic steatosis (hematoxylin & eosin staining, HE staining) and inflammatory infiltration (F4/80 staining and F4/80 gene expression). Compounds **16dk** and **16do** treatment could significantly reduce the hepatic lipid accumulation (Fig. 8A) and inflammatory infiltration (Fig. 8C) of *db/db* mice. The staining and relative expression of F4/80 of the adipose tissue in compounds-treated groups also

revealed decreased inflammation infiltration, and the irregular cell morphology seemed to be improved somewhat after treatment with **16dk** and **16do** (Fig. 8A and 8D). Meanwhile, hepatic proteins of glucose-stimulated mice were collected and western blot was performed. The serine 473 phosphorylation level of Akt (protein kinase B, PKB), as the key signaling node in hepatic insulin action was significantly elevated, suggesting the hepatic insulin resistance was ameliorated (Fig. 8B). These results indicated that compounds **16dk** and **16do** could effectively improve glucose and lipid metabolism disorder in obese diabetic *db/db* mice.

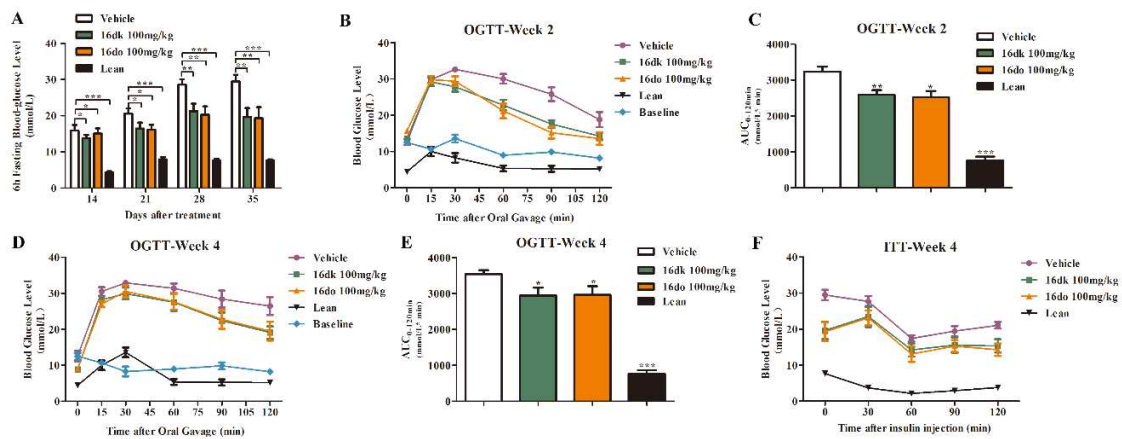


Fig. 6. Effects of compounds **16dk** and **16do** on fasting glucose level, glucose tolerance and insulin sensitivity in *db/db* mice. *db/db* and *C57* mice were treated with or without compounds **16dk** and **16do** (100 mg/kg) for 5 weeks. (A) Fasting blood glucose levels were measured regularly. (B-E) After 2- and 4-week treatment, the mice were subjected to oral glucose tolerance test (OGTT). Glucose concentrations of indicated time points and the area under curve (AUC) of OGTT were shown. (F) After 4-week treatment, mice were subjected to insulin tolerance test (ITT), the glucose curve was recorded. * $p < 0.05$, ** $p < 0.01$, *** $p < 0.001$ vs. vehicle group. Values are expressed as mean \pm S.E.M from eight independent experiments ($n = 8$ animals/group).

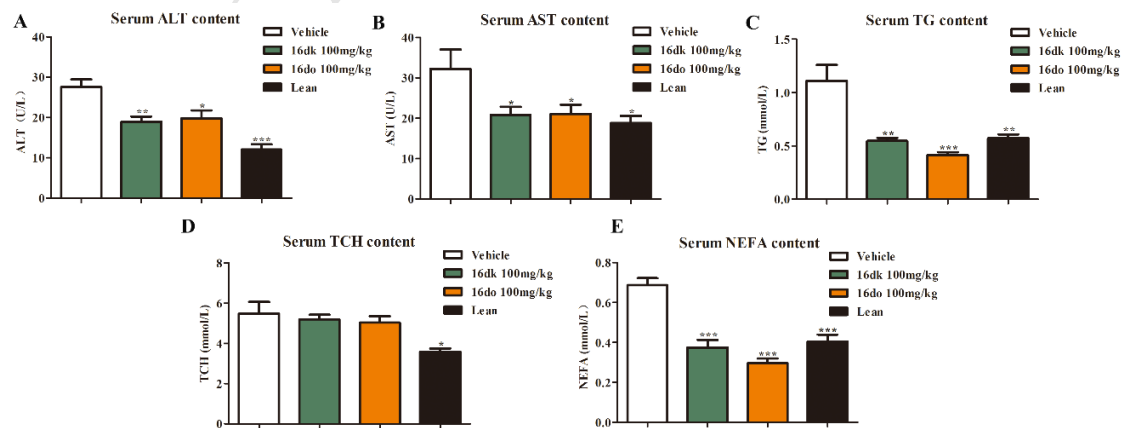


Fig. 7. Biochemical estimations of ALT, AST, TG, TCH, and NEFA in the serum. (A–E) ALT, AST, TG, TCH, and NEFA concentrations in the serum of the vehicle, compound-treated and lean groups. All indexes were measured using assay kits. * $p < 0.05$, ** $p < 0.01$, *** $p < 0.001$ vs. vehicle group. Values are given as mean \pm S.E.M from eight independent experiments ($n = 8$ animals/group).

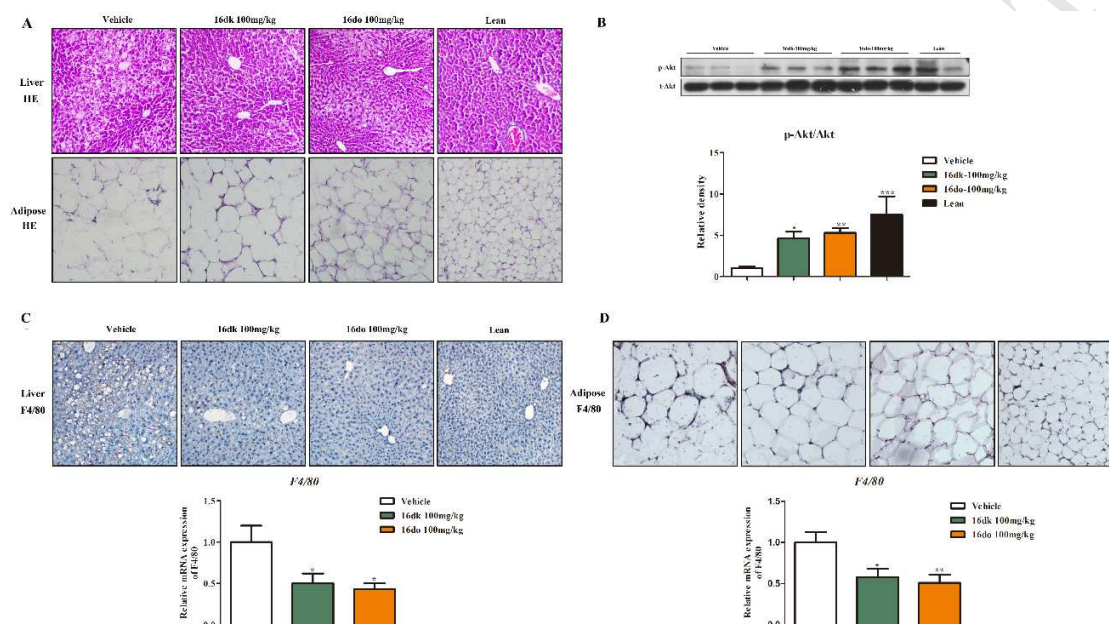


Fig. 8. Compounds **16dk** and **16do** improve liver steatosis, insulin resistance, and attenuate inflammatory infiltration of liver and adipose tissue in *db/db* mice. (A) HE staining of liver and adipose tissue. (B) Representative blots of Akt and p-Akt and histogram of the statistical results of Western blot analysis data in the liver. (C-D) Immunostaining and relative expression for F4/80 of liver (C) and adipose tissue (D). Scale bar = 100µm. * $p < 0.05$, ** $p < 0.01$, *** $p < 0.001$ versus Vehicle group. Values are given as mean \pm S.E.M from eight independent experiments ($n = 8$ animals /group).

Plasma protein binding

As animal efficacy of a compound is determined by its inhibitory activity and exposure in tissues to its unbound, or “free” fraction, the plasma protein binding experiment of compound **16dk** was conducted. As shown in the Table 7, compound **16dk** show a high plasma protein binding (98.53%) in the mouse plasma at 1µM concentration. This provide a possible reason that high plasma protein binding contribute to the high dose required in our *in vivo* study.

Table 7. The plasma protein binding rate of compound 16dk

Compd.	Species	Concentration	% Bound ^a
16dk	Mouse	1 µM	98.53%

Propranolol	Mouse	1 μ M	89.11%
--------------------	-------	-----------	--------

^a % Bound, Fraction bound; Mean percentage of three independent experiments.

Conclusion

In summary, we reported the identification of naphthalene-1-sulfonamide derivatives as novel, potent and selective FABP4 inhibitors. Systematic SAR explorations resulted in the discovery of compounds **16dk** and **16do** as potential FABP4 inhibitors for further development. In particular, crystal structures of **16dk**, **16do** and **16di** in complex with FABP4 together with the ITC study revealed the binding mode of these compounds and the importance of the water-molecule network in the binding pocket of FABP4. Furthermore, both **16dk** and **16do** showed good metabolic stabilities in liver microsomes and a dramatic improvement in glucose and lipid metabolism in *db/db* mice. All these data indicated that **16dk** and **16do** would be promising lead compounds for further development.

■ Experimental section

Chemistry methods

All reagents and solvents were purchased from commercial suppliers such as Adamas-beta®, Alfa Aesar, Acros, Bide pharmatech, etc and used without further purification unless otherwise indicated. Melting points were measured on a WRS-1B digital melting point apparatus. Flash chromatography was performed on silica gel (200–300 mesh) and visualized under UV light monitor at 254 nm. Nuclear magnetic resonance (NMR) spectroscopy were recorded with a 400 MHz Varian or a Bruker 600 MHz NMR spectrometer at ambient temperature. Chemical shifts (δ) were expressed in parts per million (ppm) downfield from tetramethylsilan, and coupling constants (J) values were described as hertz. MS was measured on Agilent 6120 quadrupole LC/MS. High resolution mass spectrometry (HRMS) determinations for all new compounds were carried out on AB SCIWX TRIPLETOF 5600+. The purity of all the tested compounds was analyzed using an Agilent 1200 HPLC system and were conformed to be $\geq 95\%$ (Table S1).

General procedure for the synthesis of intermediates **11a-11d**

To a solution of amino substituted fatty acid derivatives **10a-10d** (10 mmol) in 20 mL methanol was added thionyl chloride (20 mmol) dropwise under ice bath. After stirring at room temperature for about 2 h, the solution was evaporated to give the desired products **11a-11d**.

Methyl 4-aminobutanoate hydrochloride (**11a**)

White solid; yield 96.0 %; ¹H NMR (400 MHz, D₂O) δ 3.46 (s, 3H), 2.79 (t, J = 7.6 Hz, 2H), 2.28 (t, J = 7.3 Hz, 2H), 1.77-1.67 (m, 2H). ESI-MS: calcd for [M+H-HCl]⁺ m/z : 118.1, found: 118.1.

Methyl 3-aminopropanoate hydrochloride (11b)

White solid; yield 98.0 %; $^1\text{H NMR}$ (400 MHz, D_2O) δ 3.70 (s, 3H), 3.24 (t, $J = 6.5$ Hz, 2H), 2.78 (t, $J = 6.5$ Hz, 2H). ESI-MS: calcd for $[\text{M}+\text{H}-\text{HCl}]^+$ m/z : 104.1, found: 104.1.

Methyl 5-aminopentanoate hydrochloride (11c)

White solid; yield 95.0 %; $^1\text{H NMR}$ (400 MHz, D_2O) δ 3.64 (s, 3H), 2.95 (t, $J = 6.1$ Hz, 2H), 2.43 – 2.37 (m, 2H), 1.67 – 1.59 (m, 4H). ESI-MS: calcd for $[\text{M}+\text{H}-\text{HCl}]^+$ m/z : 132.1, found: 132.1.

Methyl 6-aminohexanoate hydrochloride (11d)

White solid; yield 96.0 %; $^1\text{H NMR}$ (400 MHz, D_2O) δ 3.44 (s, 3H), 2.74 (t, $J = 7.6$ Hz, 2H), 2.17 (t, $J = 7.4$ Hz, 2H), 1.48 – 1.34 (m, 4H), 1.21 – 1.09 (m, 2H). ESI-MS: calcd for $[\text{M}+\text{H}-\text{HCl}]^+$ m/z : 146.1, found: 146.1.

4-(3, 5-Dichlorobenzamido)butanoic acid (12)

To a solution of compound **11a** (154 mg, 1.0 mmol) in anhydrous CH_2Cl_2 (10 mL) was added 3, 5-dichlorobenzoyl chloride (209 mg, 1.0 mmol) and pyridine (241 μL 3.0 mmol) under ice bath. After stirring at room temperature for about 8 h, the solvent was removed in vacuum. The resulting residue was dissolved in NaOH (1 M) water solution (3 mL) and CH_3OH (3 mL) and stirred for another 2 h. Then the solvent was removed under vacuum, and the residue was acidified to pH = 2 or below with HCl (1 M) water solution. The solution was extracted with ethyl acetate twice and the combined organics were dried over anhydrous sodium sulfate and concentrated in vacuum. The resulting residue was purified by silica gel chromatography to give the desired compound as a white solid (234 mg, yield 85.0 %), mp 145-147 $^\circ\text{C}$. $^1\text{H NMR}$ (400 MHz, $\text{DMSO}-d_6$) δ 12.09 (s, 1H), 8.69 (t, $J = 5.3$ Hz, 1H), 7.83 (d, $J = 1.9$ Hz, 2H), 7.78 (t, $J = 1.9$ Hz, 1H), 3.27 – 3.20 (m, 2H), 2.26 (t, $J = 7.3$ Hz, 2H), 1.77 – 1.67 (m, 2H). ESI-MS: calcd for $[\text{M} - \text{H}]^-$ m/z : 274.0, found: 274.1.

4-((3, 5-Dichlorophenyl)sulfonamido)butanoic acid (14a)

The title compound was prepared from **13a** and **11a** following general procedure for the synthesis of compound **12**. White solid, yield 35.4 %, mp 169-170 $^\circ\text{C}$. $^1\text{H NMR}$ (400 MHz, $\text{DMSO}-d_6$) δ 12.12 (s, 1H), 7.99 (t, $J = 1.9$ Hz, 1H), 7.97 (s, 1H), 7.77 (d, $J = 1.9$ Hz, 2H), 2.81 (t, $J = 6.9$ Hz, 2H), 2.22 (t, $J = 7.3$ Hz, 2H), 1.64 – 1.54 (m, 2H). ESI-MS: calcd for $[\text{M} - \text{H}]^-$ m/z : 310.0, found: 310.0.

3-((3, 5-Dichlorophenyl)sulfonamido)propanoic acid (14b)

The title compound was prepared from **13a** and **11b** following general procedure for the synthesis of compound **12**. White solid, yield 39.1 %, mp 138-140 $^\circ\text{C}$. $^1\text{H NMR}$ (400 MHz, $\text{DMSO}-d_6$) δ 12.34 (s, 1H), 8.00 (s, 1H), 7.96 (t, $J = 1.9$ Hz, 1H), 7.76 (d, $J = 1.9$ Hz, 2H), 2.97 (t, $J = 6.7$ Hz, 2H), 2.36 (t, $J = 6.7$ Hz, 2H). ESI-MS: calcd for $[\text{M} - \text{H}]^-$ m/z : 296.0, found: 296.0.

5-((3, 5-Dichlorophenyl)sulfonamido)pentanoic acid (14c)

The title compound was prepared from **13a** and **11c** following general procedure for the synthesis of compound **12**. White solid, yield 45.3 %, mp 131-132 °C. ¹H NMR (400 MHz, DMSO-*d*₆) δ 12.07 (s, 1H), 7.98 (t, *J* = 1.9 Hz, 1H), 7.90 (t, *J* = 5.4 Hz, 1H), 7.77 (d, *J* = 1.9 Hz, 2H), 2.78 (dd, *J* = 11.6, 6.2 Hz, 2H), 2.16 (t, *J* = 7.2 Hz, 2H), 1.54 – 1.32 (m, 4H). ESI-MS: calcd for [M - H]⁻ *m/z* : 324.0, found: 324.0.

6-((3, 5-Dichlorophenyl)sulfonamido)hexanoic acid (14d)

The title compound was prepared from **13a** and **11d** following general procedure for the synthesis of compound **12**. White solid, yield 43.8 %, mp 130-131 °C. ¹H NMR (400 MHz, DMSO-*d*₆) δ 12.03 (s, 1H), 7.98 (t, *J* = 1.8 Hz, 1H), 7.87 (t, *J* = 5.7 Hz, 1H), 7.77 (d, *J* = 1.8 Hz, 2H), 2.77 (q, *J* = 6.7 Hz, 2H), 2.15 (t, *J* = 7.3 Hz, 2H), 1.47 – 1.32 (m, 4H), 1.27 – 1.18 (m, 2H). ESI-MS: calcd for [M - H]⁻ *m/z* : 338.0, found: 338.0.

5-((2, 4, 6-Trimethylphenyl)sulfonamido)pentanoic acid (14e)

The title compound was prepared from **13b** and **11c** following general procedure for the synthesis of compound **12**. White solid, yield 76.5 %, mp 104-105 °C. ¹H NMR (400MHz, CD₃OD) δ 7.04 (s, 2H), 2.86 (t, 2H, *J* = 6.8 Hz), 2.63 (s, 6H), 2.32 (s, 3H), 2.20 (t, 2H, *J* = 6.8Hz), 1.57 – 1.43 (m, 4H). ¹³C NMR (100MHz, CD₃OD) δ 175.8, 142.0, 138.8, 134.2, 131.5, 127.7, 123.4, 41.4, 32.8, 28.6, 23.3, 21.7, 21.6, 19.5. ESI-MS: calcd for [M - H]⁻ *m/z* : 298.1, found: 298.1.

5-((2, 3, 5, 6-Tetramethylphenyl)sulfonamido)pentanoic acid (14f)

The title compound was prepared from **13c** and **11c** following general procedure for the synthesis of compound **12**. White solid, yield 84.5 %, mp 118-121 °C. ¹H NMR (400MHz, CD₃OD) δ 7.21 (s, 1H), 2.87 (t, 2H, *J* = 6.8 Hz), 2.56 (s, 6H), 2.30 (s, 6H), 2.19 (t, 2H, *J* = 6.8), 1.60 – 1.40 (m, 4H). ¹³C NMR (100MHz, CD₃OD) δ 175.8, 142.0, 138.2, 135.8, 135.0, 134.7, 125.4, 41.4, 32.8, 28.6, 23.3, 21.6, 20.3, 19.6, 16.7. ESI-MS: calcd for [M - H]⁻ *m/z* : 312.1, found: 312.1.

5-((2, 3, 4, 5, 6-Pentamethylphenyl)sulfonamido)pentanoic acid (14g)

The title compound was prepared from **13d** and **11c** following general procedure for the synthesis of compound **12**. White solid, yield 79.3 %, mp 124-125 °C. ¹H NMR (400MHz, CD₃OD) δ 2.85 (t, 2H, *J* = 6.8), 2.58 (s, 6H), 2.31 (s, 3H), 2.27 (s, 6H), 2.17 (t, 2H, *J* = 7.2Hz), 1.60 – 1.40 (m, 4H). ¹³C NMR (100MHz, CD₃OD) δ 175.8, 139.0, 136.3, 135.0, 134.4, 133.9, 127.4, 41.5, 32.8, 28.6, 23.3, 21.6, 20.3, 17.8, 16.4, 15.7. ESI-HRMS [M - H]⁻ calcd for C₁₆H₂₄NO₄S: 326.1432, found: 326.1432.

General Procedure for the Synthesis of Intermediates 15a-15d

Substituted naphthalene (5.0 mmol) was dissolved in 15 mL of chloroform, chlorosulfonic acid (658

μL , 10.0 mmol) was added under ice bath and stirred for about 4 h at 0° C. The mixture was poured slowly into 50 mL of ice water and extracted with ethyl acetate for three times. The combined organic layer was dried over anhydrous sodium sulfate and concentrated in vacuum to give **15a-15d**, which were used directly for the next step.

5-(4-Fluoronaphthalene-1-sulfonamido)pentanoic acid (16a)

The title compound was prepared from **15a** and **11c** following general procedure for the synthesis of compound **12**. White solid, yield 85.2 %, mp 114-115 °C. ^1H NMR (400 MHz, DMSO- d_6) δ 11.95 (s, 1H), 8.69 (d, $J = 8.4$ Hz, 1H), 8.21 (d, $J = 7.9$ Hz, 1H), 8.14 (dd, $J = 8.2, 5.5$ Hz, 1H), 8.01 (t, $J = 5.7$ Hz, 1H), 7.90 – 7.73 (m, 2H), 7.49 (dd, $J = 10.1, 8.3$ Hz, 1H), 2.76 (q, $J = 6.4$ Hz, 2H), 2.04 (t, $J = 7.0$ Hz, 2H), 1.47 – 1.21 (m, 4H). ^{13}C NMR (100 MHz, DMSO- d_6) δ 174.65, 159.66, 132.56, 130.08, 129.75, 129.47, 128.11, 125.50, 124.05, 121.39, 109.14, 42.47, 33.45, 29.02, 21.94. ESI-HRMS [$\text{M} - \text{H}$] $^-$ calcd for $\text{C}_{15}\text{H}_{15}\text{FNO}_4\text{S}$: 324.0711, found: 324.0713.

5-(4-Chloronaphthalene-1-sulfonamido)pentanoic acid (16b)

The title compound was prepared from **15b** and **11c** following general procedure for the synthesis of compound **12**. White solid, yield 80.6 %, mp 158-163 °C. ^1H NMR (400 MHz, DMSO- d_6) δ 11.97 (s, 1H), 8.78 – 8.68 (m, 1H), 8.42 – 8.31 (m, 1H), 8.16 – 8.03 (m, 2H), 7.91 – 7.80 (m, 3H), 2.78 (q, $J = 6.2$ Hz, 2H), 2.05 (t, $J = 7.0$ Hz, 2H), 1.43 – 1.26 (m, 4H). ^{13}C NMR (100 MHz, DMSO- d_6) δ 174.66, 136.50, 132.20, 129.45, 129.28, 129.22, 129.19, 129.11, 128.24, 127.97, 125.96, 42.54, 33.46, 29.08, 21.94. ESI-HRMS [$\text{M} - \text{H}$] $^-$ calcd for $\text{C}_{15}\text{H}_{15}\text{ClNO}_4\text{S}$: 340.0416, found: 340.0414.

5-((4-Bromonaphthalene)-1-sulfonamido)pentanoic acid (16c)

The title compound was prepared from **15c** and **11c** following general procedure for the synthesis of compound **12**. White solid, yield 68.6 %, mp 177-179 °C. ^1H NMR (400 MHz, DMSO- d_6) δ 11.97 (s, 1H), 8.78 – 8.68 (m, 1H), 8.36 – 8.30 (m, 1H), 8.14 – 8.03 (m, 2H), 8.00 (d, $J = 7.9$ Hz, 1H), 7.90 – 7.76 (m, 2H), 2.78 (q, $J = 6.2$ Hz, 2H), 2.05 (t, $J = 7.0$ Hz, 2H), 1.43 – 1.26 (m, 4H). ^{13}C NMR (100 MHz, DMSO- d_6) δ 174.70, 136.49, 135.87, 130.95, 129.27, 129.16, 129.00, 128.93, 125.95, 125.67, 125.20, 42.54, 33.50, 29.08, 21.96. ESI-HRMS [$\text{M} - \text{H}$] $^-$ calcd for $\text{C}_{15}\text{H}_{15}\text{BrNO}_4\text{S}$: 383.9911, found: 383.9911.

5-(4-Methoxynaphthalene-1-sulfonamido)pentanoic acid (16d)

The title compound was prepared from **15d** and **11c** following general procedure for the synthesis of compound **12**. White solid, yield 56.9 %, mp 149-153 °C. ^1H NMR (400 MHz, DMSO- d_6) δ 11.96 (s, 1H), 8.59 (d, $J = 8.5$ Hz, 1H), 8.29 (d, $J = 7.8$ Hz, 1H), 8.08 (d, $J = 8.3$ Hz, 1H), 7.84 – 7.74 (m, 1H), 7.74 – 7.68 (m, 1H), 7.67 – 7.60 (m, 1H), 7.09 (d, $J = 8.4$ Hz, 1H), 4.06 (s, 3H), 2.69 (q, $J = 6.2$ Hz,

2H), 2.04 (t, $J = 7.0$ Hz, 2H), 1.43 – 1.23 (m, 4H). ^{13}C NMR (100 MHz, DMSO- d_6) δ 174.67, 158.97, 130.99, 129.23, 128.59, 127.56, 126.67, 125.75, 125.19, 122.74, 103.22, 56.68, 42.40, 33.48, 28.99, 21.99. ESI-HRMS $[\text{M} - \text{H}]^-$ calcd for $\text{C}_{16}\text{H}_{18}\text{NO}_5\text{S}$: 336.0911, found: 336.0909.

4-((4-Methoxynaphthalene)-1-sulfonamido)benzoic acid (16da)

The title compound was prepared from **15d** and methyl 4-aminobenzoate following general procedure for the synthesis of compound **12**. White solid, yield 59.9 %, mp 226-229 °C. ^1H NMR (400 MHz, DMSO- d_6) δ 12.68 (s, 1H), 11.11 (s, 1H), 8.66 (d, $J = 8.6$ Hz, 1H), 8.32 – 8.22 (m, 2H), 7.84 – 7.67 (m, 3H), 7.64 (t, $J = 7.6$ Hz, 1H), 7.16 – 7.06 (m, 3H), 4.03 (s, 3H). ^{13}C NMR (100 MHz, DMSO- d_6) δ 167.15, 159.77, 142.44, 133.06, 131.11, 129.16, 128.98, 126.94, 125.63, 125.56, 125.34, 124.53, 123.00, 117.45, 103.30, 56.80. ESI-MS: calcd for $[\text{M} - \text{H}]^-$ m/z : 356.1, found: 356.1.

2-(4-((4-Methoxynaphthalene)-1-sulfonamido)phenyl)acetic acid (16db)

The title compound was prepared from **15d** and methyl 2-(4-aminophenyl)acetate following general procedure for the synthesis of compound **12**. White solid, yield 74.1 %, mp 216-218 °C. ^1H NMR (400 MHz, DMSO- d_6) δ 12.25 (s, 1H), 10.52 (s, 1H), 8.66 (d, $J = 8.6$ Hz, 1H), 8.25 (d, $J = 8.4$ Hz, 1H), 8.18 (d, $J = 8.4$ Hz, 1H), 7.74 (t, $J = 7.6$ Hz, 1H), 7.63 (t, $J = 7.7$ Hz, 1H), 7.08 – 6.98 (m, 3H), 6.94 (d, $J = 8.4$ Hz, 2H), 4.02 (s, 3H), 3.37 (s, 2H). ^{13}C NMR (150 MHz, DMSO- d_6) δ 172.42, 158.83, 136.08, 131.86, 129.85, 128.49, 128.29, 126.17, 125.64, 124.98, 124.16, 122.27, 118.57, 102.65, 56.09. ESI-HRMS $[\text{M} - \text{H}]^-$ calcd for $\text{C}_{19}\text{H}_{16}\text{NO}_5\text{S}$: 370.0755, found: 370.0757.

4-(((4-Methoxynaphthalene)-1-sulfonamido)methyl)benzoic acid (16dc)

The title compound was prepared from **15d** and methyl 4-(aminomethyl)benzoate following general procedure for the synthesis of compound **12**. White solid, yield 63.8 %, mp 227-228 °C. ^1H NMR (400 MHz, DMSO- d_6) δ 12.87 (s, 1H), 8.60 (d, $J = 8.5$ Hz, 1H), 8.46 (t, $J = 6.2$ Hz, 1H), 8.25 (d, $J = 8.4$ Hz, 1H), 8.06 (d, $J = 8.3$ Hz, 1H), 7.76 – 7.67 (m, 3H), 7.64 (t, $J = 7.6$ Hz, 1H), 7.22 (d, $J = 8.0$ Hz, 2H), 7.02 (d, $J = 8.4$ Hz, 1H), 4.03 (d, $J = 8.4$ Hz, 5H). ^{13}C NMR (150 MHz, DMSO- d_6) δ 166.88, 158.48, 142.65, 130.60, 129.23, 128.78, 128.53, 128.02, 127.21, 126.86, 126.03, 125.10, 124.53, 122.11, 102.55, 56.06, 45.37. ESI-HRMS $[\text{M} - \text{H}]^-$ calcd for $\text{C}_{19}\text{H}_{16}\text{NO}_5\text{S}$: 370.0755, found: 370.0753.

3-((4-Methoxynaphthalene)-1-sulfonamido)benzoic acid (16dd)

The title compound was prepared from **15d** and methyl 3-aminobenzoate following general procedure for the synthesis of compound **12**. White solid, yield 63.3 %, mp 236-240 °C. ^1H NMR (400 MHz, DMSO- d_6) δ 13.00 (s, 1H), 10.82 (s, 1H), 8.67 (d, $J = 8.6$ Hz, 1H), 8.25 (d, $J = 8.4$ Hz, 1H), 8.21 (d, $J = 8.4$ Hz, 1H), 7.76 (t, $J = 7.7$ Hz, 1H), 7.67 – 7.60 (m, 2H), 7.50 – 7.44 (m, 1H), 7.32 – 7.24 (m, 2H), 7.07 (d, $J = 8.4$ Hz, 1H), 4.02 (s, 3H). ^{13}C NMR (100 MHz, CDCl_3) δ 177.83, 164.21, 141.45, 137.26,

135.23, 133.86, 133.68, 131.56, 130.99, 130.36, 129.53, 127.66, 123.93, 108.03, 61.47. ESI-MS: calcd for $[M - H]^-$ m/z : 356.1, found: 356.1.

2-(3-((4-Methoxynaphthalene)-1-sulfonamido)phenyl)acetic acid (16de)

The title compound was prepared from **15d** and methyl 2-(3-aminophenyl)acetate following general procedure for the synthesis of compound **12**. White solid, yield 59.0 %, mp 170-174 °C. ^1H NMR (400 MHz, acetone- d_6) δ 9.26 (s, 1H), 8.75 (d, $J = 8.6$ Hz, 1H), 8.29 (d, $J = 8.4$ Hz, 1H), 8.26 (d, $J = 8.4$ Hz, 1H), 7.69 (t, $J = 7.7$ Hz, 1H), 7.59 (t, $J = 7.5$ Hz, 1H), 7.16 (s, 1H), 7.06 (t, $J = 7.8$ Hz, 1H), 6.99 (d, $J = 8.3$ Hz, 2H), 6.90 (d, $J = 7.4$ Hz, 1H), 4.06 (s, 3H), 3.47 (s, 2H). ^{13}C NMR (150 MHz, DMSO- d_6) δ 172.12, 158.86, 137.63, 135.73, 132.01, 128.70, 128.51, 128.29, 126.15, 125.58, 125.00, 124.16, 124.15, 122.25, 119.33, 116.54, 102.61, 56.08, 40.50. ESI-HRMS $[M - H]^-$ calcd for $\text{C}_{19}\text{H}_{16}\text{NO}_5\text{S}$: 370.0755, found: 370.0751.

3-(((4-Methoxynaphthalene)-1-sulfonamido)methyl)benzoic acid (16df)

The title compound was prepared from **15d** and methyl 3-(aminomethyl)benzoate following general procedure for the synthesis of compound **12**. White solid, yield 51.2 %, mp 200-205 °C. ^1H NMR (400 MHz, DMSO- d_6) δ 8.54 (d, $J = 8.6$ Hz, 1H), 8.41 (t, $J = 6.3$ Hz, 1H), 8.21 (d, $J = 8.2$ Hz, 1H), 8.05 (d, $J = 8.3$ Hz, 1H), 7.70-7.62 (m, 2H), 7.58 (t, $J = 7.5$ Hz, 1H), 7.29 (d, $J = 7.6$ Hz, 1H), 7.20 (t, $J = 7.6$ Hz, 1H), 7.00 (d, $J = 8.4$ Hz, 1H), 4.01 (s, 3H), 3.99 (d, $J = 6.1$ Hz, 2H). ^{13}C NMR (100 MHz, DMSO- d_6) δ 167.04, 158.59, 138.13, 131.79, 130.73, 130.35, 128.59, 128.30, 128.12, 128.05, 127.78, 126.96, 126.11, 125.19, 124.58, 122.22, 102.64, 56.14, 45.43. ESI-HRMS $[M - H]^-$ calcd for $\text{C}_{19}\text{H}_{16}\text{NO}_5\text{S}$: 370.0755, found: 370.0756.

3-(1-((4-Methoxynaphthalene)-1-sulfonamido)ethyl)benzoic acid (16dg)

The title compound was prepared from **15d** and methyl 3-(1-aminoethyl)benzoate following general procedure for the synthesis of compound **12**. White solid, yield 59.7 %, mp 218-221 °C. ^1H NMR (400 MHz, DMSO- d_6) δ 8.48 (d, $J = 8.6$ Hz, 1H), 8.40 (d, $J = 8.4$ Hz, 1H), 8.12 (d, $J = 8.5$ Hz, 1H), 7.95 (d, $J = 8.3$ Hz, 1H), 7.66 – 7.58 (m, 1H), 7.57 – 7.44 (m, 2H), 7.18 (d, $J = 7.8$ Hz, 1H), 7.04 – 6.96 (m, 1H), 6.89 (d, $J = 8.5$ Hz, 1H), 4.31 – 4.21 (m, 1H), 3.97 (s, 3H), 1.11 (d, $J = 6.8$ Hz, 3H). ^{13}C NMR (100 MHz, DMSO- d_6) δ 167.02, 158.50, 143.24, 130.91, 130.12, 130.05, 128.51, 127.91, 127.65, 127.37, 127.00, 126.76, 125.92, 124.98, 124.52, 122.08, 102.45, 56.03, 52.43, 23.24. ESI-HRMS $[M - H]^-$ calcd for $\text{C}_{20}\text{H}_{18}\text{NO}_5\text{S}$: 384.0911, found: 384.0911.

3-(3-((4-Methoxynaphthalene)-1-sulfonamido)phenyl)propanoic acid (16dh)

The title compound was prepared from **15d** and methyl 3-(3-aminophenyl)propanoate following general procedure for the synthesis of compound **12**. White solid, yield 60.9 %, mp 161-162 °C. ^1H

NMR (400 MHz, DMSO- d_6) δ 10.27 (s, 1H), 8.44 (d, J = 8.7 Hz, 1H), 8.02 (d, J = 8.5 Hz, 1H), 7.98 (d, J = 8.4 Hz, 1H), 7.51 (t, J = 7.5 Hz, 1H), 7.40 (t, J = 7.6 Hz, 1H), 6.86 – 6.74 (m, 2H), 6.67 (s, 1H), 6.60 – 6.50 (m, 2H), 3.80 (s, 3H), 2.41 (t, J = 7.5 Hz, 2H), 2.14 (t, J = 7.5 Hz, 2H). ^{13}C NMR (150 MHz, DMSO- d_6) δ 173.34, 158.85, 141.65, 137.63, 132.03, 128.74, 128.52, 128.27, 126.14, 125.60, 124.97, 124.18, 123.05, 122.23, 118.35, 116.20, 102.61, 56.08, 34.71, 29.97. ESI-HRMS $[\text{M} - \text{H}]^-$ calcd for $\text{C}_{20}\text{H}_{18}\text{NO}_5\text{S}$: 384.0911, found: 384.0913.

2-Fluoro-3-((4-methoxynaphthalene)-1-sulfonamido)benzoic acid (16di)

The title compound was prepared from **15d** and methyl 3-amino-2-fluorobenzoate following general procedure for the synthesis of compound **12**. White solid, yield 53.3 %, mp 235-236 °C. ^1H NMR (400 MHz, DMSO- d_6) δ 10.53 (s, 1H), 8.64 (d, J = 8.6 Hz, 1H), 8.25 (d, J = 8.2 Hz, 1H), 8.05 (d, J = 8.4 Hz, 1H), 7.74 – 7.66 (m, 1H), 7.66-7.59 (m, 1H), 7.53-7.46 (m, 1H), 7.45-7.38 (m, 1H), 7.12 (t, J = 8.0 Hz, 1H), 7.01 (d, J = 8.5 Hz, 1H), 4.00 (s, 3H). ^{13}C NMR (100 MHz, DMSO- d_6) δ 164.51, 159.12, 155.24, 152.65, 131.61, 128.80, 128.61, 128.39, 127.85, 126.40, 125.97, 125.79, 125.13, 124.44, 124.11, 122.35, 102.73, 56.25. ESI-HRMS $[\text{M} - \text{H}]^-$ calcd for $\text{C}_{18}\text{H}_{13}\text{FNO}_5\text{S}$: 374.0504, found: 374.0500.

3-((4-Methoxynaphthalene)-1-sulfonamido)-2-methylbenzoic acid (16dj)

The title compound was prepared from **15d** and methyl 3-amino-2-methylbenzoate following general procedure for the synthesis of compound **12**. White solid, yield 65.8 %, mp 183-187 °C. ^1H NMR (400 MHz, DMSO- d_6) δ 12.90 (s, 1H), 9.87 (s, 1H), 8.64 (d, J = 8.5 Hz, 1H), 8.27 (d, J = 8.3 Hz, 1H), 7.92 (d, J = 8.3 Hz, 1H), 7.69 (t, J = 7.3 Hz, 1H), 7.66 – 7.60 (m, 1H), 7.46 (d, J = 7.4 Hz, 1H), 7.07 (t, J = 7.8 Hz, 1H), 7.02 – 6.96 (m, 2H), 4.01 (s, 3H), 2.07 (s, 3H). ^{13}C NMR (100 MHz, DMSO- d_6) δ 168.80, 158.86, 135.91, 134.77, 133.07, 131.30, 129.43, 128.72, 128.25, 127.57, 126.89, 126.35, 125.81, 125.16, 124.66, 122.35, 102.81, 56.24, 14.97. ESI-HRMS $[\text{M} - \text{H}]^-$ calcd for $\text{C}_{19}\text{H}_{16}\text{NO}_5\text{S}$: 370.0755, found: 370.0754.

2-Fluoro-5-((4-methoxynaphthalene)-1-sulfonamido)benzoic acid (16dk)

The title compound was prepared from **15d** and methyl 5-amino-2-fluorobenzoate following general procedure for the synthesis of compound **12**. White solid, yield 50.8 %, mp 220-222 °C. ^1H NMR (400 MHz, DMSO- d_6) δ 10.71 (s, 1H), 8.61 (d, J = 8.6 Hz, 1H), 8.23 (d, J = 8.3 Hz, 1H), 8.12 (d, J = 8.4 Hz, 1H), 7.74 (t, J = 7.3 Hz, 1H), 7.62 (t, J = 7.6 Hz, 1H), 7.47 (dd, J = 6.2, 2.7 Hz, 1H), 7.24 – 7.16 (m, 1H), 7.13 – 7.06 (m, 1H), 7.03 (d, J = 8.5 Hz, 1H), 3.99 (s, 3H). ^{13}C NMR (100 MHz, DMSO- d_6) δ 164.36, 159.17, 158.58, 156.06, 133.77, 132.17, 128.61, 128.51, 126.45, 125.09, 124.11, 122.48, 122.09, 119.48, 117.86, 117.62, 102.78, 56.27. ESI-HRMS $[\text{M} - \text{H}]^-$ calcd for $\text{C}_{18}\text{H}_{13}\text{FNO}_5\text{S}$: 374.0504,

found: 374.0505.

5-((4-Methoxynaphthalene)-1-sulfonamido)-2-methylbenzoic acid (16dl)

The title compound was prepared from **15d** and methyl 5-amino-2-methylbenzoate following general procedure for the synthesis of compound **12**. White solid, yield 35.1 %, mp 214-217 °C. ¹H NMR (400 MHz, DMSO-*d*₆) δ 12.83 (s, 1H), 10.58 (s, 1H), 8.64 (d, *J* = 8.7 Hz, 1H), 8.23 (d, *J* = 8.4 Hz, 1H), 8.13 (d, *J* = 8.3 Hz, 1H), 7.73 (t, *J* = 7.8 Hz, 1H), 7.60 (t, *J* = 7.9 Hz, 1H), 7.46 (d, *J* = 1.8 Hz, 1H), 7.10-7.02 (m, 3H), 4.00 (s, 3H), 2.29 (s, 3H). ¹³C NMR (100 MHz, DMSO-*d*₆) δ 168.06, 159.04, 135.45, 133.87, 132.15, 131.08, 128.56, 126.39, 125.40, 125.10, 124.25, 122.51, 121.84, 122.35, 120.64, 102.77, 56.27, 20.44. ESI-HRMS [M - H]⁻ calcd for C₁₉H₁₆NO₅S: 370.0755, found: 370.0754.

3-Fluoro-5-((4-methoxynaphthalene)-1-sulfonamido)benzoic acid (16dm)

The title compound was prepared from **15d** and methyl 3-amino-5-fluorobenzoate following general procedure for the synthesis of compound **12**. White solid, yield 54.8 %, mp 247-249 °C. ¹H NMR (400 MHz, DMSO-*d*₆) δ 11.14 (s, 1H), 8.61 (d, *J* = 8.6 Hz, 1H), 8.27-8.21 (m, 2H), 7.75 (t, *J* = 7.8 Hz, 1H), 7.62 (t, *J* = 7.6 Hz, 1H), 7.43 (s, 1H), 7.17 (d, *J* = 8.7 Hz, 1H), 7.10-7.02 (m, 2H), 4.01 (s, 3H). ¹³C NMR (100 MHz, DMSO-*d*₆) δ 165.57, 163.14, 160.71, 159.40, 133.70, 132.46, 128.77, 128.43, 126.53, 125.15, 124.74, 123.94, 122.56, 114.77, 110.08, 108.57, 102.84, 56.32. ESI-HRMS [M - H]⁻ calcd for C₁₈H₁₃FNO₅S: 374.0504, found: 374.0505.

3-Chloro-5-((4-methoxynaphthalene)-1-sulfonamido)benzoic acid (16dn)

The title compound was prepared from **15d** and methyl 3-amino-5-chlorobenzoate following general procedure for the synthesis of compound **12**. White solid, yield 43.6 %, mp 223-226 °C. ¹H NMR (400 MHz, DMSO-*d*₆) δ 11.13 (s, 1H), 8.61 (d, *J* = 8.6 Hz, 1H), 8.27 – 8.20 (m, 2H), 7.80 – 7.73 (m, 1H), 7.66-7.60 (m, 1H), 7.56 (t, *J* = 1.7 Hz, 1H), 7.40 (t, *J* = 1.7 Hz, 1H), 7.25 (t, *J* = 2.0 Hz, 1H), 7.10 (d, *J* = 8.5 Hz, 1H), 4.02 (s, 3H). ¹³C NMR (100 MHz, DMSO-*d*₆) δ 165.45, 159.43, 139.59, 133.62, 133.55, 132.47, 128.81, 128.43, 126.57, 125.16, 124.75, 124.06, 123.17, 122.68, 121.03, 117.19, 102.88, 56.37. ESI-HRMS [M - H]⁻ calcd for C₁₈H₁₃ClNO₅S: 390.0208, found: 390.0212.

4-Fluoro-3-((4-methoxynaphthalene)-1-sulfonamido)benzoic acid (16do)

The title compound was prepared from **15d** and methyl 3-amino-4-fluorobenzoate following general procedure for the synthesis of compound **12**. White solid, yield 62.5 %, mp 228-230 °C. ¹H NMR (400 MHz, DMSO-*d*₆) δ 13.11 (s, 1H), 10.57 (s, 1H), 8.65 (d, *J* = 8.6 Hz, 1H), 8.25 (d, *J* = 8.3 Hz, 1H), 8.02 (d, *J* = 8.4 Hz, 1H), 7.86-7.80 (m, 1H), 7.74-7.68 (m, 1H), 7.67 – 7.59 (m, 2H), 7.20 – 7.11 (m, 1H), 7.02 (d, *J* = 8.5 Hz, 1H), 4.01 (s, 3H). ¹³C NMR (150 MHz, DMSO-*d*₆) δ 165.72, 159.05, 158.36, 156.67, 131.42, 128.52, 128.24, 127.84, 127.22, 126.27, 125.77, 125.02, 124.76, 124.30, 122.22,

116.17, 102.58, 56.15. ESI-HRMS [M - H]⁻ calcd for C₁₈H₁₃FNO₅S: 374.0504, found: 374.0504.

4-Chloro-3-((4-methoxynaphthalene)-1-sulfonamido)benzoic acid (16dp)

The title compound was prepared from **15d** and methyl 3-amino-4-chlorobenzoate following general procedure for the synthesis of compound **12**. White solid, yield 53.3 %, mp 235-239 °C. ¹H NMR (400 MHz, DMSO-*d*₆) δ 13.23 (s, 1H), 10.35 (s, 1H), 8.65 (d, *J* = 8.5 Hz, 1H), 8.25 (d, *J* = 7.6 Hz, 1H), 7.98 (d, *J* = 8.4 Hz, 1H), 7.83 (s, 1H), 7.71-7.65 (m, 1H), 7.65-7.59 (m, 2H), 7.40 (d, *J* = 8.3 Hz, 1H), 7.01 (d, *J* = 8.5 Hz, 1H), 4.01 (s, 3H). ¹³C NMR (100 MHz, DMSO-*d*₆) δ 165.93, 159.13, 134.03, 133.09, 131.40, 130.14, 130.14, 128.74, 128.23, 127.61, 127.23, 126.36, 126.36, 125.15, 124.80, 122.34, 102.70, 56.26. ESI-HRMS [M - H]⁻ calcd for C₁₈H₁₃ClNO₅S: 390.0208, found: 390.0213.

4-Methyl-3-((4-methoxynaphthalene)-1-sulfonamido) benzoic acid (16dq)

The title compound was prepared from **15d** and methyl 3-amino-4-methylbenzoate following general procedure for the synthesis of compound **12**. White solid, yield 51.0 %, mp 233-236 °C. ¹H NMR (400 MHz, DMSO-*d*₆) δ 12.81 (s, 1H), 9.91 (s, 1H), 8.65 (d, *J* = 8.5 Hz, 1H), 8.26 (d, *J* = 8.2 Hz, 1H), 7.94 (d, *J* = 8.4 Hz, 1H), 7.69 (t, *J* = 7.4 Hz, 1H), 7.66 – 7.59 (m, 2H), 7.55 (d, *J* = 7.8 Hz, 1H), 7.12 (d, *J* = 7.9 Hz, 1H), 6.99 (d, *J* = 8.4 Hz, 1H), 4.02 (s, 3H), 1.90 (s, 3H). ¹³C NMR (100 MHz, DMSO-*d*₆) δ 166.65, 158.92, 145.78, 138.70, 135.20, 131.40, 130.82, 129.00, 128.66, 128.27, 126.69, 126.64, 126.37, 125.15, 124.62, 122.46, 102.76, 56.24, 17.78. ESI-HRMS [M - H]⁻ calcd for C₁₉H₁₆NO₅S: 370.0755, found: 370.0759.

4-Methoxy-3-((4-methoxynaphthalene)-1-sulfonamido)benzoic acid (16dr)

The title compound was prepared from **15d** and methyl 3-amino-4-methoxybenzoate following general procedure for the synthesis of compound **12**. White solid, yield 53.7 %, mp 229-231 °C. ¹H NMR (400 MHz, DMSO-*d*₆) δ 12.70 (s, 1H), 9.78 (s, 1H), 8.69 (d, *J* = 8.5 Hz, 1H), 8.24 (d, *J* = 8.4 Hz, 1H), 7.91 (d, *J* = 8.4 Hz, 1H), 7.78 (d, *J* = 2.1 Hz, 1H), 7.72 – 7.66 (m, 1H), 7.65 – 7.59 (m, 2H), 6.96 (d, *J* = 8.5 Hz, 1H), 6.82 (d, *J* = 8.7 Hz, 1H), 3.99 (s, 3H), 3.18 (s, 3H). ¹³C NMR (100 MHz, DMSO-*d*₆) δ 166.61, 158.80, 155.83, 131.09, 128.91, 128.23, 127.95, 126.65, 126.19, 125.89, 125.37, 125.07, 125.05, 122.72, 122.06, 111.15, 102.46, 56.22, 55.29. ESI-HRMS [M - H]⁻ calcd for C₁₉H₁₆NO₆S: 386.0704, found: 386.0708.

2-((4-Methoxynaphthalene)-1-sulfonamido)isonicotinic acid (16ds)

The title compound was prepared from **15d** and methyl 2-aminoisonicotinate following general procedure for the synthesis of compound **12**. White solid, yield 33.7 %, mp 294-297 °C. ¹H NMR (400 MHz, DMSO-*d*₆) δ 8.67 (d, *J* = 8.6 Hz, 1H), 8.27 (d, *J* = 8.4 Hz, 1H), 8.22 (d, *J* = 8.3 Hz, 1H), 8.11 (d, *J* = 4.7 Hz, 1H), 7.71 (t, *J* = 7.4 Hz, 1H), 7.59 (t, *J* = 7.5 Hz, 1H), 7.52 (s, 1H), 7.19 (d, *J* = 4.5 Hz,

1H), 7.10 (d, $J = 8.5$ Hz, 1H), 4.02 (s, 3H). ^{13}C NMR (100 MHz, DMSO- d_6) δ 165.45, 158.87, 153.01, 140.98, 131.76, 128.68, 128.34, 126.96, 126.23, 125.08, 124.59, 122.41, 115.57, 112.89, 111.71, 102.74, 56.27. ESI-HRMS $[\text{M} - \text{H}]^-$ calcd for $\text{C}_{17}\text{H}_{13}\text{N}_2\text{O}_5\text{S}$: 357.0551, found: 357.0554.

5-((4-Methoxynaphthalene)-1-sulfonamido)nicotinic acid (16dt)

The title compound was prepared from **15d** and methyl 5-aminonicotinate following general procedure for the synthesis of compound **12**. White solid, yield 45.5 %, mp 252-255 °C. ^1H NMR (400 MHz, DMSO- d_6) δ 13.49 (s, 1H), 11.13 (s, 1H), 8.64-8.58 (m, 2H), 8.41 (d, $J = 2.5$ Hz, 1H), 8.27-8.20 (m, 2H), 7.87 (t, $J = 2.0$ Hz, 1H), 7.76 (t, $J = 7.7$ Hz, 1H), 7.63 (t, $J = 7.7$ Hz, 1H), 7.08 (d, $J = 8.5$ Hz, 1H), 4.02 (s, 3H). ^{13}C NMR (100 MHz, DMSO- d_6) δ 165.63, 159.43, 144.73, 143.31, 134.59, 132.46, 128.82, 128.40, 126.72, 126.58, 125.63, 125.15, 124.70, 123.96, 122.67, 102.91, 56.35. ESI-HRMS $[\text{M} - \text{H}]^-$ calcd for $\text{C}_{17}\text{H}_{13}\text{N}_2\text{O}_5\text{S}$: 357.0551, found: 357.0551.

2, 4-Difluoro-5-((4-methoxynaphthalene)-1-sulfonamido)benzoic acid (16du)

The title compound was prepared from **15d** and methyl 5-amino-2, 4-difluorobenzoate following general procedure for the synthesis of compound **12**. White solid, yield 60.8 %, mp 211-214 °C. ^1H NMR (400 MHz, DMSO- d_6) δ 10.47 (s, 1H), 8.61 (d, $J = 8.5$ Hz, 1H), 8.26 (d, $J = 8.0$ Hz, 1H), 7.96 (d, $J = 8.4$ Hz, 1H), 7.72-7.60 (m, 3H), 7.24 (t, $J = 10.3$ Hz, 1H), 7.00 (d, $J = 8.5$ Hz, 1H), 4.00 (s, 3H). ^{13}C NMR (100 MHz, DMSO- d_6) δ 163.57, 159.17, 157.81, 157.70, 131.60, 129.55, 128.65, 128.37, 126.39, 125.71, 125.12, 124.41, 122.35, 121.11, 115.68, 106.05, 102.71, 56.27. ESI-HRMS $[\text{M} - \text{H}]^-$ calcd for $\text{C}_{18}\text{H}_{12}\text{F}_2\text{NO}_5\text{S}$: 392.0410, found: 392.0411.

2, 6-Difluoro-3-((4-methoxynaphthalene)-1-sulfonamido)benzoic acid (16dv)

The title compound was prepared from **15d** and methyl 3-amino-2, 6-difluorobenzoate following general procedure for the synthesis of compound **12**. White solid, yield 53.9%, mp 211-214 °C. ^1H NMR (400 MHz, DMSO- d_6) δ 10.44 (s, 1H), 8.60 (d, $J = 8.5$ Hz, 1H), 8.26 (d, $J = 7.9$ Hz, 1H), 8.00 (d, $J = 8.4$ Hz, 1H), 7.74-7.68 (m, 1H), 7.67-7.60 (m, 1H), 7.31 – 7.19 (m, 1H), 7.07 (t, $J = 8.7$ Hz, 1H), 7.01 (d, $J = 8.5$ Hz, 1H), 4.01 (s, 3H). ^{13}C NMR (100 MHz, DMSO- d_6) δ 161.56, 159.16, 155.01, 154.08, 131.58, 128.78, 128.62, 128.39, 126.41, 125.87, 125.15, 124.39, 122.38, 121.43, 112.58, 112.08, 102.75, 56.27. ESI-HRMS $[\text{M} - \text{H}]^-$ calcd for $\text{C}_{18}\text{H}_{12}\text{F}_2\text{NO}_5\text{S}$: 392.0410, found: 392.0408.

***In vitro* FABPs inhibition assay**

The inhibitory activities of the compounds against FABPs were measured in a fluorescence-based assay using the probe 8-anilino-1-naphthalene-sulfonic acid (1, 8-ANS) [29,30]. Briefly, 10 $\mu\text{mol/L}$ of 1, 8-ANS in 0.01M phosphate buffered solution (PBS, pH 7.4) was mixed with FABPs protein to a final concentration of 10 $\mu\text{mol/L}$, then various concentrations of compounds were added and

incubated for 3 min at room temperature. The fluorescence signal at 370 nm (excitation) / 470 nm (emission) of the reaction mixture was then determined with a Flexstation III instrument (Molecular Devices, CA, USA). The IC₅₀ value for compounds against FABPs were expressed as mean ± standard deviation (SD) of three independent experiments, and calculated by nonlinear regression using GraphPad Prism software (San Diego, CA, USA). K_i values were calculated according to the equation in Jacobs et al [34]. K_d values were determined as 1.4 μM by Scatchard plot analysis using recombinant human FABP4 protein. Compound **1** was purchased from APEX BIO Technology, Houston, USA. Compound **2** was synthesized in-house according to reference 21. Each compound was tested in triplicate and the data are presented as the mean ± SD.

X-ray protein structure determination

Expression, purification, and crystallization of recombinant human FABP4 are described in the Supporting Information. Crystals of complexes were obtained via soaking apo-FABP4 crystals with 2 mM compounds in mother liquor overnight. The protocol for data collection and data determination is described in the Supporting Information.

Isothermal titration calorimetry (ITC)

The ITC measurements were conducted at 30 °C with ITC200 instrument (Microcal, GE Healthcare), and the resulting data were processed by the supplied MicroCal Origin software package. Before titration, the stock solution of **16di** or **16do** was diluted to the concentration of 500 μM and 1 mM, respectively. The FABP4 was diluted to 50-150 μM. The final concentration of DMSO in the reaction buffer is 2.5% of the total volume. Titration of the compound into FABP4 was performed using an initial injection of 0.44 μL followed by 19 identical injections of 2 μL with a duration of 4 seconds per injection and a spacing of 120 seconds between injections. The last ten data points were averaged and subtracted from each titration to account for the heat of dilution (inhibitor into protein). Additional background experiments where buffer was titrated into the protein solution revealed no significant shift in the baseline during the course of the measurements. Titrations were run in triplicate to ensure reproducibility. In all cases, a single binding site mode was employed and a nonlinear least-squares algorithm was used to obtain change in enthalpy (ΔH) and binding constant (K). Thermodynamic parameters were subsequently calculated with the formula $\Delta G = \Delta H - T\Delta S = -RT \ln K$ and $K_d = 1/K$, where T, R, ΔG , ΔS and K_d are the experimental temperature, the gas constant, the changes in free energy, the entropy of binding, and the dissociation constant, respectively.

Oil red O staining and triglyceride assay

Compounds **16dk** or **16do** (50 μM) were added at the beginning of 3T3-L1 differentiation induction

and incubated in the medium throughout the differentiation period (day 0-6), respectively. At day 6, cells were washed in PBS and then fixed for 15 min at 37°C with 4% paraformaldehyde. Cells were then washed twice with PBS and stained with Oil-Red-O solution (0.5% isopropanol-dissolved Oil Red O dye: water = 3:2; AMRESCO) for 30min, after staining, the cells were washed with PBS and observed by Olympus's fluorescent inverted microscope (OLYMPUS IX73). For quantification, Oil-Red-O dye was dissolved in isopropanol and absorbance at 500 nm was measured by a FlexStation3 system (Molecular Devices, Sunnyvale, CA, USA). For intracellular TG measurement, cells were washed and lysed as previously reported.³⁵ Briefly, cells were lysed with three repeated freeze-thaw cycle(-80°C and 37°C) and then triglyceride content was determined by a commercial enzyme assay kit (Mingdian, Shanghai, China).

Lipolysis assay

For forskolin-stimulated lipolysis, fully differentiated 3T3-L1 cells were cultured with DMEM for 4 h followed by incubation with compounds **16dk** or **16do** (25 µM and 50 µM) for 24 h. Then the cells were washed twice with Krebs-Ringer Hepes buffer (KRBH buffer, 135 mM NaCl, 3.6mM KCl, 0.5 mM KH₂PO₄, 0.5 mM MgSO₄, 2 mM NaHCO₃, 1.5 mM CaCl₂, and 10 mM HEPES, pH7.4) containing 0.1% BSA and stimulated with 20 µM forskolin diluted in KRBH buffer for 2 h. Thereafter culture supernatants were assayed for glycerol levels using a free glycerol reagent kit (Applygen Technologies Inc, China).

Liver microsomal stability assay

The tested compound (final concentration 0.1 µM, co-solvent (0.01% DMSO) and 0.005% Bovin serum albumin) was incubated with 0.33 mg/mL indicated liver microsomes (liver microsomes of rats and humans were purchased from BD Gentest; liver microsomes of mouse were purchased from RILD). NADPH was maintained at 1 mM in 450 µL of reaction volume. The reaction was then evaluated at 0, 7, 17, 30 and 60 min and was terminated by the addition of methanol. Samples were centrifuged for 5 min at 15000 rpm and the supernatants were analyzed using HPLC-MS/MS. Percentage parent remaining was calculated considering percent parent area at 0 min as 100%.

Animal experiment

Male C57BL/KsJ-*db/db* mice and their lean littermates were obtained from Jackson Laboratories (Bar Harbor, ME, USA) and maintained in a 12 h light-dark cycle with regular chow diet and free access to water. Male mice at 6 weeks of age were randomly divided into 4 groups (n = 8 per group). Then, they were given daily by lavage administration with the vehicle (0.5% carboxymethyl cellulose), **16dk** (100 mg/kg of body weight), and **16do** (100 mg/kg of body weight). Meanwhile, their lean littermates

were treated with vehicle in the same way as normal control. Body weight was recorded regularly. Every week, each group of mice were fasted for 6 h before their blood glucose were monitored using tail vein blood with a glucometer (Accu-CHEK, Roche). On week 2 and week 4 post-drug administration, the mice were fasted for 12 h and 6 h respectively to perform oral glucose tolerance test (OGTT) and insulin tolerance test (ITT) as previously described [36]. Briefly, for OGTT, the mice were fasted overnight and given an oral glucose load (0.5 g/kg) by gavage. The blood glucose was measured in the tail vein using glucometer at 0, 15, 30, 60, 90, and 120 min, the curve of blood glucose was plotted, and the area under curve (AUC) was calculated. For ITT, after 6 h fasting, the mice were given insulin (1 IU/kg) via intraperitoneal injection, and the blood glucose was measured at 0, 30, 60, 90min, and 120 min, the curve of blood glucose and the AUC were obtained. At the end of the experimental period, the blood samples and tissue samples were collected for following analysis. Serum ALT, AST, TG and TCH levels were assayed according to the kit instructions with commercial enzyme assay kits (Mingdian, Shanghai, China). Serum non-esterified fatty acid was also measured using assay kit (Jiancheng, Nanjing, China). All animal experiments were permitted by the Institutional Animal Care and Use Committee of Shanghai Institute of Materia Medica (accreditation number: 2015-01-WHY-13).

Histomorphology and Immunohistochemistry

Tissue samples were fixed in a 4% buffered paraformaldehyde solution immediately after dissection, then embedded in paraffin wax, cut into 5 μm -thick sections and stained with Hematoxylin and Eosin Staining Kit (Beyotime, Shanghai, China). For immunohistochemistry, F4/80 staining was performed in liver and adipose sections using the rabbit polyclonal F4/80 antibody (Santa Cruz Biotechnology) and MaxVision™ HRP-Polymer anti-Mouse/Rabbit IHC Kit (Maixin, Fuzhou, China) as a visualization of macrophages infiltration. Briefly, tissue sections were washed in phosphate-buffered saline and incubated overnight at 4 °C with F4/80 antibody (1:50) and then treated with MaxVision™ HRP-Polymer anti-Mouse/Rabbit IHC Kit for 15min at room temperature followed by incubation with diaminobenzidine. The slides were counterstained with hematoxylin and images were captured using Olympus's fluorescent inverted microscope (OLYMPUS IX73).

Western blot analysis

Mouse liver tissues were lysed in RIPA Lysis Buffer (Beyotime, China) and clarified by centrifugation (Eppendorf, Germany). Lysates were separated by SDS-PAGE, transferred to a PVDF membrane, probed with primary antibodies and detected with secondary antibodies. The primary antibodies used were Akt Antibody and Phospho-Akt (Ser473) Antibody (Cell Signaling Technology, USA, 1:1000),

and the secondary antibodies used were anti-rabbit IgG (Jackson Laboratory, USA, 1:10000). The blots were then visualized using chemiluminescence (ECL) detection reagents (Thermo Fisher Scientific). Data were analyzed by integrated optical density and the relative density ratio of p-Akt was adjusted to Akt and normalized to Vehicle group.

Gene expression analysis

Total RNA were extracted from liver and adipose tissue surrounding testis using TRIzol reagent (Invitrogen, USA) according to the manufacturer's instructions. For gene expression analysis, the cDNA was obtained from total RNA using All-in-One cDNA Synthesis SuperMix (Biomake, China) according to the manufacturer's instructions. mRNA levels were quantified by real-time PCR using SYBR Green qPCR Master Mix (Biomake, China) and an ABI VIIA7 Real-Time PCR machine (Applied Biosystems, USA) according to the manufacturer's instructions. The amplification program was as follows: initial denaturation at 95°C for 5 min (Hold Stage), followed by 40 cycles of 95°C for 15 s, 60°C for 45s (PCR Stage), and 95°C for 15 s, 60°C for 1min, 95°C for 15 s (Melt Curve Stage). The primer sequences were as follows: b-actin (forward: CCACGATGGAGGGGCCGACTCATC, and reverse: CTAAAGACCTCTATGCCAACACAGT), F4/80 (forward: TGACTCACCTTGTGGTCCTAA, and reverse: CTTCCCAGAATCCAGTCTTTCC). The relative expression level of F4/80 from liver and adipose tissue was normalized to the amount of b-actin mRNA.

Statistical analysis

Statistical analysis of different groups was assessed by t test or one-way analysis of variance (ANOVA) followed by Dunnett's test analysis, and a value of $p < 0.05$ was considered significant.

Molecular modeling

The crystal structure of FABP4 in complex with palmitic acid was obtained from PDB Protein Data Bank (PDB code 2HNX) for docking simulation. The protein was prepared with Protein Preparation Wizard panel in Maestro 10.0. After adding the missing hydrogen atom, all the crystallographic water molecules were removed. Then the protein was submitted to several restrained minimization to relieve static clashes using OPLS2005 force field. At last, the protein was adjusted and minimized up to 0.30 Å RMSD. The size of grid box was defined as 15 Å × 15 Å × 15 Å centered in the co-crystal ligand using Receptor Grid Generation. Compounds for docking were built using 2D Sketcher and were prepared with LigPrep module. Molecular docking was conducted using glide module with standard precision scoring (SP) mode. The Fig.s were generated using Pymol [37].

Plasma protein binding

Plasma protein binding was performed as described by Reck et al [38].

■ Acknowledgments

This work was supported by grants from National Natural Science Foundation of China (Grant 81473075 to Y.-X.L., Grant 81473262 to H.-Y.W., and Grant 81422047 to Y.-C.X.), the National Key R&D Program of China (Grant 2016YFA0502301 to W.-L.Z. and Y.-C.X.), Institutes for Drug Discovery and Development, Chinese Academy of Sciences (Grant CASIMM0120164014 to H.-Y.W.) and the State Key Laboratory of Drug Research (Grant SIMM1803KF-05 to Y.-X.L.)

■ Abbreviations

FABP, Fatty Acid Binding Protein; SAR, Structure–activity relationship; 3-D Three-dimensional; IGF-1, Insulin-like growth factors -1; 1, 8-ANS, 8-anilino-1-naphthalene-sulfonic acid; PDB, Protein Data Bank; ITC, Isothermal titration calorimetry; DMF, dimethylformamide; DMEM, Dulbecco's modified eagle medium; FBS, Fetal bovine serum; MTT, Thiazolyl blue tetrazolium bromide ; DMSO, dimethyl sulfoxide; KRBH buffer, Krebs-Ringer Hepes buffer; PBS ,Phosphate-Buffered Saline; OGTT, Oral glucose tolerance test; ITT, Insulin tolerance test; AUC, Area under curve; ALT, Alanine aminotransferase; AST, Aspartate transaminase; TG, Triglyceride; NEFA, Non-esterified fatty acid; TCH, Total cholesterol; HE staining, Hematoxylin & Eosin staining. GPR40, Free fatty acid receptor 1; GPR120, Free fatty acid receptor 4; DGAT1, Acyl coenzyme A: diacylglycerol acyltransferase 1; PPAR γ , Peroxisome proliferator activated receptor γ .

Appendix A. Supplementary data

Supplementary data include supplementary Fig.s, HPLC analysis of all target compounds, protein expression and purification, crystal structure and determination, cell culture and cell proliferation assay

Supplementary data related to this article can be found at

References

- [1] G.S. Hotamisligil, Inflammation and metabolic disorders, *Nature* 444 (2006) 860-867.
- [2] M. Furuhashi, G.S. Hotamisligil, Fatty acid-binding proteins: role in metabolic diseases and potential as drug targets, *Nat. Rev. Drug Discov.* 7 (2008) 489-503.
- [3] G.S. Hotamisligil, D.A. Bernlohr, Metabolic functions of FABPs—mechanisms and therapeutic implications, *Nat Rev Endocrinol.* 11 (2015) 592-605.
- [4] R.K. Ockner, J.A. Manning, R.B. Poppenhausen, W.K. Ho, A binding protein for fatty acids in cytosol of intestinal mucosa, liver, myocardium, and other tissues, *Science* 177 (1972) 56-58.
- [5] J. Storch, A.E. Thumser, Tissue specific functions in the fatty acid-binding protein family, *J Biol*

Chem. 285 (2010) 32679-3268.

[6] R.Z. Liu, X. Li, R. Godbout, A novel fatty acid-binding protein (FABP) gene resulting from tandem gene duplication in mammals: transcription in rat retina and testis, *Genomics* 92 (2008) 436-445.

[7] A.V. Hertzler, D.A. Bernlohr, The mammalian fatty acid-binding protein multigene family: molecular and genetic insights into function, *Trends Endocrinol. Metab.* 11 (2000) 175-180.

[8] A. Chmurzyńska, The multigene family of fatty acid-binding proteins (FABPs): function, structure and polymorphism, *J. Appl. Genet.* 47 (2006) 39-48.

[9] S.A. Melki, N.A. Abumrad, Expression of the adipocyte fatty acid-binding protein in streptozotocin-diabetes: effects of insulin deficiency and supplementation, *J. Lipid Res.* 34 (1993) 1527-1534.

[10] R.J. Distel, G.S. Robinson, B.M. Spiegelman, Fatty acid regulation of gene expression. *J. Biol. Chem.* 267 (1992) 5937-5941.

[11] L. Makowski, J.B. Boord, K. Maeda, V.R. Babaev, K.T. Uysal, M.A. Morgan, R.A. Parker, J. Suttles, S. Fazio, G.S. Hotamisligil, M.F. Linton, Lack of macrophage fatty-acid-binding protein aP2 protects mice deficient in apolipoprotein E against atherosclerosis, *Nat. Med.* 7 (2001) 699-705.

[12] C.R. Hunt, J.H. Ro, D.E. Dobson, H.Y. Min, B.M. Spiegelman, Adipocyte P2 gene: developmental expression and homology of 50-flanking sequences among fat cell-specific genes. *Proc. Natl. Acad. Sci. U. S. A.* 83 (1986) 3786-3790.

[13] G.S. Hotamisligil, R.S. Johnson, R.J. Distel, R. Ellis, V.E. Papaioannou, B.M. Spiegelman, Uncoupling of obesity from insulin resistance through a targeted mutation in aP2, the adipocyte fatty acid binding protein. *Science* 274 (1996) 1377-1379.

[14] K.T. Uysal, L. Scheja, S.M. Wiesbrock, S. Bonner-Weir, G.S. Hotamisligil, Improved glucose and lipid metabolism in genetically obese mice lacking aP2. *Endocrinology* 141 (2000) 3388-3396.

[15] (a) N.R. Coe, M.A. Simpson, D.A. Bernlohr, Targeted disruption of the adipocyte lipid-binding protein (aP2 protein) gene impairs fat cell lipolysis and increases cellular fatty acid levels. *J. Lipid Res.* 40 (1999) 967-972. (b) T. Garin-Shkolnik, A. Rudich, G.S. Hotamisligil, M. Rubinstein, FABP4 attenuates PPAR γ and adipogenesis and is inversely correlated with PPAR γ in adipose tissues. *Diabetes* 63 (2014) 900-911.

[16] (a) K.M. Nieman, H.A. Kenny, C.V. Penicka, A. Ladanyi, R. Buell-Gutbrod, M.R. Zillhardt, I.L. Romero, M.S. Carey, G.B. Mills, G.S. Hotamisligil, S.D. Yamada, M.E. Peter, K. Gwin, E. Lengyel, Adipocytes promote ovarian cancer metastasis and provide energy for rapid tumor growth, *Nat. Med.*

- 17 (2011) 1498-1503. (b) H. Uehara, T. Takahashi, M. Oha, H. Ogawa, K. Izumi, Exogenous fatty acid binding protein 4 promotes human prostate cancer cell progression, *Int. J. Cancer* 135 (2014) 2558-2568. (c) A. Tolle, S. Suhail, M. Jung, K. Jung, C. Stephan, Fatty acid binding proteins (FABPs) in prostate, bladder and kidney cancer cell lines and the use of ILFABP as survival predictor in patients with renal cell carcinoma, *BMC Cancer* 11 (2011) 302. (d) D. Lee, K. Wada, Y. Taniguchi, H. Al-Shareef, T. Masuda, Y. Usami, T. Aikawa, M. Okura, Y. Kamisaki, M. Kogo, Expression of fatty acid binding protein 4 is involved in the cell growth of oral squamous cell carcinoma, *Oncol. Rep.* 31 (2014) 1116-1120. (e) S.A. Abdelwahab, Y. Owada, N. Kitanaka, A. Adida, H. Sakagami, M. Ono, M. Watanabe, F. Spener, H. Kondo, Enhanced expression of adipocyte-type fatty acid binding protein in murine lymphocytes in response to dexamethasone treatment, *Mol. Cell. Biochem.* 299 (2007) 99-107. (f) S. Guaita-Esteruelas, J. Guma, L. Masana, J. Borrás, The peritumoural adipose tissue microenvironment and cancer. The roles of fatty acid binding protein 4 and fatty acid binding protein, *Mol. Cell. Endocrinol.* 462 (2018) 107-118. (g) S. Guaita-Esteruelas, A. Bosquet, P. Saavedra, J. Guma, J. Girona, E.W. Lam, K. Amillano, J. Borrás, L. Masana, Exogenous FABP4 increases breast cancer cell proliferation and activates the expression of fatty acid transport proteins, *Mol. Carcinog.* 56 (2017) 208-217. (h) F. Yan, N. Shen, J.X. Pang, Y.W. Zhang, E.Y. Rao, A.M. Bode, A. Al-Kali, D.E. Zhang, M.R. Litzow, B. Li, S.J. Liu, Fatty acid-binding protein FABP4 mechanistically links obesity with aggressive AML by enhancing aberrant DNA methylation in AML cells. *Leukemia* 31 (2017) 1434 - 1442.
- [17] Y. Shen, G. Song, Y. Liu, L. Zhou, H. Liu, X. Kong, Y. Sheng, K. Cao, L. Qian, Silencing of FABP3 inhibits proliferation and promotes apoptosis in embryonic carcinoma cells, *Cell Biochem. Biophys.* 66 (2013) 139-146.
- [18] Y. Liu, G. Song, H. Liu, X. Wang, Y. Shen, L. Zhou, J. Jin, M. Liu, C. Shi, L. Qian, Silencing of FABP3 leads to apoptosis-induced mitochondrial dysfunction and stimulates Wnt signaling in zebrafish, *Mol. Med. Rep.* 8 (2013) 806-812.
- [19] X. Wang, L. Zhou, J. Jin, Y. Yang, G. Song, Y. Shen, H. Liu, M. Liu, C. Shi, L. Qian, Knockdown of FABP3 impairs cardiac development in zebra fish through the retinoic acid signaling pathway, *Int. J. Mol. Sci.* 14 (2013) 13826-13841.
- [20] (a) M. Furuhashi, G. Tuncman, C.Z. Görgün, L. Makowski, G. Atsumi, E. Vaillancourt, K. Kono, V.R. Babaev, S. Fazio, M.F. Linton, R. Sulsky, J.A. Robl, R.A. Parker, G.S. Hotamisligil, Treatment of diabetes and atherosclerosis by inhibiting fatty-acid-binding protein aP2, *Nature* 447 (2007) 959-965. (b) T. Okada, M. Hiromura, M. Otsuka, S. Enomoto, H. Miyachi, Synthesis of BMS-309403-related

compounds, including [¹⁴C]BMS-309403, a radioligand for adipocyte fatty acid binding protein, *Chem. Pharm. Bull.* 60 (2012) 164-168.

[21] H. Kühne, U. Obst-Sander, B. Kuhn, A. Conte, S.M. Ceccarelli, W. Neidhart, M.G. Rudolph, G. Ottaviani, R. Gasser, S.S. So, S. Li, X. Zhang, L. Gao, M. Myers, Design and synthesis of selective, dual fatty acid binding protein 4 and 5 inhibitors, *Bioorg. Med. Chem. Lett.* 26 (2016) 5092-5097.

[22] T. Barf, F. Lehmann, K. Hammer, S. Haile, E. Axen, C. Medina, J. Uppenberg, S. Svensson, L. Rondahl, T. Lundback, N-Benzyl-indolo carboxylic acids: design and synthesis of potent and selective adipocyte fatty-acid binding protein (AFABP) inhibitors, *Bioorg. Med. Chem. Lett.* 19 (2009) 1745-1748.

[23] R. Ringom, E. Axen, J. Uppenberg, T. Lundback, L. Rondahl, T. Barf, Substituted benzylamino-6-(trifluoromethyl)pyrimidin-4(1H)-ones: a novel class of selective human A-FABP inhibitors, *Bioorg. Med. Chem. Lett.* 14 (2004) 4449-4452.

[24] A.V. Hertz, K. Hellberg, J.M. Reynolds, A.C. Kruse, B.E. Juhlmann, A.J. Smith, M.A. Sanders, D.H. Ohlendorf, J. Suttles, D.A. Bernlohr, Identification and characterization of a small molecule inhibitor of Fatty Acid binding proteins, *J. Med. Chem.* 52 (2009) 6024-6031.

[25] R. Sulsky, D.R. Magnin, Y. Huang, L. Simpkins, P. Taunk, M. Patel, Y. Zhu, T.R. Stouch, D. Bassolino-Klimas, R. Parker, T. Harrity, R. Stoffel, D.S. Taylor, T.B. Lavoie, K. Kish, B.L. Jacobson, S. Sheriff, L.P. Adam, W.R. Ewing, J.A. Robl, Potent and selective biphenyl azole inhibitors of adipocyte fatty acid binding protein (aFABP), *Bioorg. Med. Chem. Lett.* 17 (2007) 3511-3515.

[26] H. Cai, Q. Liu, D. Gao, T. Wang, T. Chen, G. Yan, K. Chen, Y. Xu, H. Wang, Y. Li, W. Zhu, Novel fatty acid binding protein 4 (FABP4) inhibitors: virtual screening, synthesis and crystal structure determination, *Eur. J. Med. Chem.* 90 (2015) 241-250.

[27] H. Cai, G. Yan, X. Zhang, O. Gorbenko, H. Wang, W. Zhu, Discovery of highly selective inhibitors of human fatty acid binding protein4 (FABP4) by virtual screening, *Bioorg. Med. Chem. Lett.* 20 (2010) 3675-3679.

[28] G. Floresta, V. Pistrà, E. Amata, M. Dichiarà, A. Marrazzo, O. Prezzavento, A. Rescifina, Adipocyte fatty acid binding protein 4 (FABP4) inhibitors. A comprehensive systematic review, *Eur. J. Med. Chem.* 138 (2017) 854-873.

[29] H.Y. Cai, T. Wang, J.C. Zhao, P. Sun, G.R. Yan, H.P. Ding, Y.X. Li, H.Y. Wang, W.L. Zhu, K.X. Chen, Benzbromarone, an old uricosuric drug, inhibits human fatty acid binding protein 4 in vitro and lowers the blood glucose level in db/db mice, *Acta Pharmacol Sin.* 34 (2013) 1397-1402.

[30] C.D. Kane, D.A. Bernlohr, A simple assay for intracellular lipid-binding proteins using

- displacement of 1-anilinoanthracene 8-sulfonic acid, *Anal Biochem.* 233 (1996) 197-204.
- [31] J. Cramer, S.G. Krimmer, A. Heine, G. Klebe, Paying the price of desolvation in solvent-exposed protein pockets: impact of distal solubilizing groups on affinity and binding thermodynamics in a series of thermolysin inhibitors, *J. Med. Chem.* 60 (2017) 5791-5799.
- [32] S.G. Krimmer, J. Cramer, M. Betz, V. Fridh, R. Karlsson, A. Heine, G. Klebe, Rational design of thermodynamic and kinetic binding profiles by optimizing surface water networks coating protein-bound ligands, *J. Med. Chem.* 59 (2016) 10530-10548.
- [33] Y. Wang, H.Q. Lin, W.K. Law, W.C. Liang, J.F. Zhang, J.S. Hu, T.M. Ip, M.M. Waye, D.C. Wan, Pimozide, a novel fatty acid binding protein 4 inhibitor, promotes adipogenesis of 3T3-L1 cells by activating PPAR γ , *ACS Chem. Neurosci.* 6 (2015) 211-218.
- [34] J. Steven, C. Kwen-Jen, C. Pedro, Estimation of hormone receptor affinity by competitive displacement of labeled ligand: effect of concentration of receptor and of labeled ligand, *Biochem. Biophys. Res. Commun.* 66 (1975) 687-692.
- [35] X. Zhang, J. Ji, G. Yan, J. Wu, X. Sun, J. Shen, H. Jiang, H. Wang, Sildenafil promotes adipogenesis through a PKG pathway, *Biochem. Biophys. Res. Commun.* 396 (2010) 1054-1059.
- [36] J. Zhu, J. Huang, T. Wang, J. Ji, A. Hou, H. Wang, Sanggenol F exerts anti-diabetic effects via promoting adipocyte differentiation and modifying adipokines expression, *Endocrine* 56 (2017) 73-81.
- [37] W.L. Delano, *The PyMOL molecular graphics system*, version 1.7.0; Schrödinger, LLC: New York, 2014.
- [38] F. Reck, R. Alm, P. Brassil, J. Newman, B. Dejonge, C.J. Eyermann, G. Breault, J. Breen, J. Comita-Prevoir, M. Cronin, H. Davis, D. Ehmann, V. Galullo, B. Geng, T. Grebe, M. Morningstar, P. Walker, B. Hayter, S. Fisher, Novel N-linked aminopiperidine inhibitors of bacterial topoisomerase type II: broad-spectrum antibacterial agents with reduced hERG activity, *J. Med. Chem.* 54 (2011) 7834-7847.

Highlights:

1. Compounds **16dk** and **16do** were discovered as selective FABP4 inhibitors using a structure-based design strategy.
2. The X-ray crystal structures revealed the binding mode of compounds **16d**, **16dk**, **16do**, **16di** with FABP4.
3. A systematic study was performed to validate the efficacy of **16dk** and **16do** both *in vitro* and *in vivo*.